Luminescent ions in advanced composite materials for multifunctional applications

Gongxun Bai, Ming-Kiu Tsang, and Jianhua Hao*

G. X. Bai, M.-K. Tsang, Prof. J. H. Hao

Department of Applied Physics,The Hong Kong Polytechnic University, Hong Kong, P. R. China

The Hong Kong Polytechnic University Shenzhen Research Institute, Shenzhen, P. R. China

E-mail: jh.hao@polyu.edu.hk

Keywords: metal ion dopants; luminescence; upconversion nanocrystals; composites; multifunctional applications.

Abstract

Luminescent ions doped materials have been widely applied in many areas, both scientific research and practical fields. Recently, incorporating luminescent ions and advanced materials into versatile and multifunctional systems seems to be a tendency, motivated by the stimulating desires of fundamental studies and technological applications. This feature article provides a general overview of the myriad of luminescent ions-based advanced composite materials recently investigated. It is demonstrated that the improved or additional properties may be achieved via implementing a strategy of incorporating luminescent ions (lanthanide, transition and main group metal ions) into various types of materials, such as flexible polymers, two-dimensional atomically thin layers, porous materials and so on. We outline the

design principles, synthesis and processing of various systems joined by luminescent ions doped phosphors. A number of recent works indicate that those novel composite materials allow one to conceive and develop multifunctional applications in a broad area, including optoelectronics, photonics, clean energy, biomedicine, and new types of sensors. Lastly, some challenging issues are discussed and potential directions are suggested for further developing advanced composite materials incorporated with luminescent ions.

1. Introduction

Luminescence is a phenomenon in which the excitation energy of a substance excited by external energy is given off as photon, resulting in the form of light emission. Here light consists of not only electromagnetic waves in the visible range between 390 and 700 nm, but also those in ultraviolet (UV) and near-infrared (NIR) spectra.[1] Luminescence has been playing a major scientific and technological role for humankind. A large group of widely used luminescent materials also called phosphors, is composed of luminescent ions namely activators and a suitable host, named as metal-ion-doped phosphors. [2] To date, studies on metal-ion-doped phosphors have covered almost all branches of luminescence. Numerous kinds of metal-ion-doped phosphors have been synthesized in different forms, such as glasses, crystal bulks, powders, nanoparticles (NPs), [3] and thin films, [4] in which the luminescence properties primarily depend on the energy transition of luminescent ions. Mostly, three kinds of metal ions may serve as activators, namely, lanthanide (Ln) ions, transition metal (TM) ions, and main group metal ions. [5] The resulted luminescence attributed to metal ion dopants can cover a broad range of optical spectra, including UV, visible, and NIR regions. Accordingly, such luminescent features make metal-ion-doped phosphors maintain their dominant position in the phosphors used for widespread application from optoelectronics to biomedicine, through to approximately every aspect of human life.

It is noticeable that the ability to fabricate or tune materials to acquire improved or multifunctional properties is highly desired in the materials science community. It has become a conventional strategy in a variety of research fields to combine two or more different compounds, or materials into a composite form while maintaining the beneficial aspects of each constituent. Recently, numerous emerged advanced materials, such as NPs and two dimensional (2D) materials, have been widely studied.[6] It is an important approach to combine luminescent ion doped phosphors with those advanced novel materials, aiming at optimizing the performance and processing of optical materials. [7] The formed composites not only complement different functional properties in one system, but also highly offer a possibility to manufacture high-performance and low-cost materials. For instance, the composite materials associated with Ln dopants, such as upconversion/magnetic luminescence and porous with multifunctional properties have recently been reported. [8]

The study of luminescent ions in composite materials is not limited to fundamental interests in materials. Moreover, these modified materials with potential coupling effects are also promising for multifunctional applications, including novel display, multimodal bioimaging, phototherapy, drug delivery, biodetection, photocatalysis, and optical sensing. In principle, these composite materials may possess superior mechanical, luminescent, or thermal properties, and possess a better processability than the single system of phosphors in multifunctional application. One group of these kinds of composite materials is organic and organic-inorganic metal-ion doped hybrid phosphors, such as metal-organic frameworks. Note that some reviews associated with this area regarding organic materials have already been published, and interested readers can refer to these references.[9] Here, we will mainly focus on the combination of recently advanced emerging materials with luminescent ions doped phosphors. Up to now, there has been no specific review to provide a comprehensive coverage of the progress in the novel types of luminescent composites. This feature article is set out as follows. Further to this section of instruction, we will present the fundamentals of

several luminescent ions and considerations of the related composite material design in Section 2. Furthermore, Section 3 will describe the synthesis of advanced composite materials incorporated with luminescent ions, while Section 4 will highlight the applications of luminescent ions in advanced composite materials. Finally, we will conclude with perspectives.

2. Luminescent ions in advanced composite materials

2.1. Principles of luminescent ions

Luminescent ions are generally capable of responding to photon excitation and subsequently emitting light, also called photoluminescence (PL). Depending on the decay time (r) of photon emission, PL can be classified as fluorescence and phosphorescence. Fluorescence possesses a short time lapse (r <10 ms) after the excitation source is removed, whereas phosphorescence has a much longer decay time (r >0.1 s). [10] According to the fundamental mechanisms, the luminescence of active ions can be basically classified into several types. As shown in **Figure 1**, the emissions of luminescent ions include (a) down-shifting, (b) down-conversion, and (c) upconversion. Down-shifting and -conversion processes feature Stokes emissions with photon energy smaller than the excitation source. One kind of down-conversion emissions is called quantum cutting, meaning an excitation photon to generate two or more low energy photons. Upconversion luminescence is an anti-Stokes emission which needs two or more excitation photons to produce a higher energy photon. In case of an active ion without efficient absorption matching the available pump energy, a sensitizer ion can be incorporated into the host material to transfer the excitation energy to the activator (Figure 1 (d)). As shown in Figure 1 (e), when luminescent ions are doped semiconductor host, emission can occur under band-to-band excitation. The excitation energy transfers from the semiconductor host to the doped luminescent ions. On the whole, luminescent ions can absorb the supplied energy and then give specific light due to the

variation in the energy-level structure. As mentioned above, luminescent ions mainly include lanthanide, transition metal, and main group metal ions. **Figure 2** shows the luminescent ions highlighted in a periodic table. Their typical luminescent ions and their emissions corrosponded to energy transitions are listed in **Table 1**. [11-25]

The Ln series contain 15 metallic ions, from lanthanum (atomic number 57) to lutetium (atomic number 71). Besides La^{3+} being equivalent to Xe in electronic configuration, the Ln ions characterized by a partly filled 4*f* shell are shielded from their surroundings by the filled $5s^2$ and $5p^6$ orbitals, giving rise to a weak electron-phonon coupling and resulting in narrow and sharp emission lines of 4*f*-4*f* transitions.[26] In comparison, the emission bands originating from 5*d*-4*f* transitions (*e.g.*, Ce^{3+}) are broad, because the 5*d* electrons are unshielded and hence greatly influenced by their surroundings. The emission lifetimes of 4*f*-4*f* transitions are substantially long-lived, typically in the range of milliseconds because of the forbidden character of *f*-*f* transitions in free 4*f* ions. In cases where luminescence arises from parity-allowed transitions, such as 5*d*-4*f* transitions, a much shorter lifetime (~10^{-5} s) is recorded.[4] Due to their abundant ladderlike energy levels, Ln ions, such as Er^{3+}, Eu^{3+}, Nd^{3+}, Ho^{3+}, Tm^{3+} and Pr^{3+}, have been widely studied as active ions for luminescent materials. [27] To date, Ln^{3+}-doped phosphors have demonstrated amazing down-conversion and upconversion luminescence covering from UV to NIR region. For example, Er^{3+} ion is well-documented and most extensively used luminescent dopant for the following reasons. Its characteristic emission at 1.55 μm matches the minimum attenuation of silica optical fibers mostly used in optical fiber communication. In addition, the red and green emissions correspond to 4*f* transitions of $^4F_{9/2}$ $^4I_{15/2}$ and $^2H_{11/2}/^4S_{3/2}$ $^4I_{15/2}$ of Er^{3+} ions, respectively.[28] Hence, visible emissions ascribed to Er^{3+} ions have widely been utilized in optical sensor, display and bioprobe. On the other hand, phosphors containing Eu^{3+} ions can display superior red emission around 616 nm. The characteristic emission bands of Eu^{3+} ion in hosts are located at around 579, 593, 614, 652 and 705 nm, corresponding to $^5D_0$ ^7F_j transitions (j =0, 1, 2, 3,

and 4). [29] Nd^{3+} ions can present NIR emissions at 800, 870, 946, 1064, and 1320 nm, respectively. [30]

Besides Ln ions, TM ion is another kind of mostly recognized luminescent ions. [31] In history, the luminescence of Cr^{3+} doped Al_2O_3 was utilized for the first generation of solid-state lasers. In general, TM ions have a partly filled *d*-shell (d^n, $0<n<10$). [32] The 3*d* TM ions utilized in phosphors have three electrons (Cr^{3+} and Mn^{4+}), or five electrons (Mn^{2+} and Fe^{3+}), occupying the outermost 3*d* orbitals. In contrast to lanthanide ions, the 3*d* orbitals are not shielded from the host lattice. Thus, the energy level structures of TM ions are sensitive to their coordination environment. Environmental perturbations, including chemical or structural modifications, can lead to the changes in bond lengths, bond angles, covalence, and coordination number. As a result, the luminescence of TM ions is featured by broad and undefined characteristics. Specifically, with an increase in crystal field strength, the emission between $^4T_1$ and $^6A_1$ can shift from green to deep red. For instance, Mn^{2+}-doped ZnS with orange emission is one of typical phosphors in PL and electroluminescence (EL) applications. [33] Another interesting phenomenon is the observation of broadband NIR luminescence from Ni^{2+}-doped phosphors. The NIR luminescence of Ni^{2+} ions can be modified by fine-tuning the crystal field strength through chemical ways or strain engineering. [34]

Apart from lanthanide ions and TM ions, main group metal ions containing 6*p* (Bi, Pb) and 5*p* (Sb, Sn, In, Te), are promising as a new type of active ion, due to the broadband NIR luminescence originating from the unsheltered outer 6*s* or 6*p* electron transitions. [35] In particular, Bi-doped phosphors have drawn much attention due to their ultrabroadband NIR luminescence, covering the whole windows of optical fiber communications. [36]

2.2. Materials design

In the past decades, phosphors based on luminescent ions have played a vital role in various applications, including solid-state lasers, fiber communication, display devices, solid state

lighting, and biomedicine. To realize more opportunities for luminescent ions, readily scalable composite material is important alternatives to be fabricated into a new material platform for further investigation through a coupling approach. Incorporating luminescent ions into several advanced functional materials while keeping the beneficial aspects of each component can form novel multifunctional materials. **Figure 3** shows the considerations of material design to fabricate advanced composite materials with luminescent dopants. Through incorporating the luminescent ions with some advanced materials, improved or multifunctional properties of the prepared composite enable to be applied in many applications, including novel type of display, optical sensing, multimodal bioimaging, biodetection, photocatalysis, etc. [37]

In general, there are several material selections for designing advanced functional composite materials. As summarized in **Table 2**, some functional materials, including polymers, magnetic materials, porous materials, catalysts, and 2D materials, can be considered to combine with the luminescent ion phosphors. [38-42] And some new merits could be added to the luminescent ions. As a typical example, when mixing the luminescent materials into polymer polydimethylsiloxane (PDMS) matrix, the synthesized composite usually possesses useful properties of flexible, easy processabilty, and low-cost compared to traditional regid inorganic hosts doped with luminescent ions. The prepared composite can be processed as optical waveguides on wafers for photonic application. Additionally, both magnetic and luminescence properties can be realized in a two-phase system consisted of magenetic materials (Fe_3O_4, etc.) and luminescent ions doped phosphors. And then the luminescence of the fabricated composite may be modulated by magnetic field. The prepared composite with the multifunctional properties can be considered in some areas, such as biomedicine and magnetic sensors.

3. Synthesis and characterizations of various materials

In this section, the synthesis of luminescent ions in advanced composite materials will be introduced as a sequence of the combining materials.

3.1. Polymer matrix composite

A variety of polymers are popular materials in research and industry, even in our daily life. Broadly, polymers possess significant characteristics of corrosion resistance, low density, or electrical insulating behavior. In polymer matrix composite, the polymer forms a continuous phase in which the luminescent ion doped component can be embedded. The latter is usually present as the form of NPs or microparticles, or fibers. The processabilty and diversity of polymers together with remarkable luminescent properties of inorganic luminescent ion doped phosphors make them highly possible to fabricate high-performance and low-cost photonic and optoelectronic devices or systems. [43] In order to fabricate polymer matrix composites, either particles or fibers or the polymer matrix or all components can be prepared either *in situ* or *ex situ*. [44]

In situ fabrication of luminescent ions doped phosphor particles in polymer matrix is a simple route to prepare the composites. Mixing of the precursor components can proceed in a polymer melt. In such processes, the conversion of the precursors to the final luminescent ions doped inorganic particles can take place in solutions, polymer melts or polymeric solids. This method allows one-step preparation of luminescent composites with *in situ* generated phosphor particles from corresponding precursors. In this case, the particles can be synthesized inside the selected polymer matrix. The benefit of this method is that it avoids particle agglomeration while keeping a good spatial distribution in the polymer matrix. The drawback of this route is that the unreacted educts of the *in situ* reaction might influence the physical properties of the final composite material.

Another main approach for the fabrication of polymer matrix composite is to disperse pre-prepared luminescent ions doped particles directly into polymers. This route is defined as *ex*

situ preparation of luminescent ions doped composites. The *ex situ* preparation is more suitable for large-scale application. For example, metal-ion-doped ZnS microparticles were uniformly dispersed into PDMS matrix to produce a flexible phosphor composite, as shown in **Figure 4** (a).[45] ZnS is an excellent semiconductor with non-symmetrical crystal structure, giving rise to inner piezoelectric potential when applying external strain. Metal-ions-doped ZnS can present different colors, depending on the energy transitions of various dopants. Typically, ZnS doped with Cu and Mn (ZnS:Cu,Mn) or Cu (ZnS:Cu), can emit orange and green colors, respectively. PDMS can be selected as a matrix to encapsulate the metal-ion-doped ZnS microparticles and also transfer external stimuli to the luminescent centers. PDMS features high flexibility, high optical transparent, durable, and low cost characteristics, which has extensively been utilized in the fields of flexible biological sensor, solar cell, and piezoelectric nanogenerators. The prepared flexible phosphor composite can be either used individually or coated on arbitrary substrates. More interestingly, multiple stimuli, including electric field, photon, various types of strains (pressure, friction, etc.) can trigger the fabricated luminescent composites and therefore generate light. As shown in Figure 4 (b), when dispersing the rare-earth-ions doped nanocrystals into the KMPR® polymer, the nanocrystal-doped KMPR polymer composite can be fabricated for the optical waveguide.[46] The KMPR® polymer combined with luminescent ions doped nanocrystals was spin-coated on a silicon substrate with 6 μm thick silicon dioxide layer and pre-annealed at 90 °C for 5 min. Then, the waveguide channels were defined by the photo mask under UV exposure. Post-annealing of 2 min at 90 °C was applied to solidify the polymer. Finally, waveguides with dimensions of 11 mm height and 13 mm width were prepared by standard photolithography.

3.2. Combining with 2D materials

Nowadays, graphene and graphene-like 2D atomic materials have been considered promising candidates for next-generation electronics and optoelectronics devices, owing to their amazing structural, electrical and optical properties. Graphene is one of the thinnest materials ever made. It's 100 times stronger than steel, a better heat and electrical conductor than copper, flexible, and largely transparent. [47] In contrast to gapless graphene, a variety of 2D layered semiconductors have bandgaps. In particular, 2D-layered transition metal dichalcogenides (TMDs) present a desirable luminescence, a high current on/off ratio in field-effect transistors (FETs). Researchers envision a future for 2D materials in everything from the potential applications of electronics, photonics, and energy to biomedicine. [48]

Mostly, the luminescent ions doped 2D materials are *in situ* prepared. For instance, taking the benefit of the rather large surface area of TMDs nanosheets, metal-ion- doped WS_2 nanoflakes were fabricated for cancer theranostics.[49] As shown in **Figure 5** (a), a WCl_6:MCl_x (M= Fe, Co, Ni, Mn, and Gd) mixture at desired ratios was added into the pre-mixed solvent of 20 mL oleylamine and 10 mL 1-octadecene at room temperature. And then the solution was heated to remove oxygen and water under vigorous magnetic stirring in the present protection of nitrogen. Afterward, the temperature of the solution was fast raised up to 300 °C and sulfurized with sulfur solution. Finally, metal-ions-doped WS_2 nanoflakes with polyethylene glycol (PEG) modification can be employed as multifunctional agents for biomedicine. In addition, 2D graphene nanosheets can also be utilized as scaffolds for the assembly of luminescent ions doped upconversion nanocrystals, as shown in Figure 5 (b).[50] An example for the composite of luminescent ions in graphene-like materials is the synthesis of $NaYF_4$:Yb,Er-graphene oxide (GO) multifunctional composite materials by *in situ* growth of luminescent ions doped NPs in the existence of GO.[51] In this process, GO was mixed with the precursor components, and the conversion of the precursors to the final luminescent ions doped NPs can take place in solutions. Since GO is rich in hydroxyl and carboxylic groups, it can coordinate with rare earth ions to form a complex.[52]

3.3. Grafting into porous materials

Porous materials are good choices for fabricating luminescent composite materials. Porous materials are known to compose small pores, in which the surface area can be largely increased. As a result, porous materials are ideal matrix to load different types of luminescent materials with high capturing density to meet the needs for diverse applications. Very recently, our group fabricated a hybrid material by anchoring amine functionalized upconversion NPs (UCNPs) into the hollow channels of nanoporous anodized alumina membrane (NAAO) to form hybrid structure for subsequent biological application.[53] Amine is a popular surface group for biological application because it can be readily linked to different types of biological species.[54] The anchoring process was initiated via etching hydrogen peroxide followed by surface salinization. Then, the UCNPs are linked by glutaraldehyde to the surface of the NAAO channels (**Figure 6** (a)). In addition to NAAO, the luminescent NPs can be combined with porous polystyrene (PS) microspheres.[55] The preparation of the composite is relatively simple when considering the attraction of the PS microspheres and UCNPs is based on hydrophobic-hydrophobic interaction (Figure 6 (b)).[56] Therefore, the incubation of swelled PS microspheres and oleate-UCNPs in organic solvent is sufficient for forming the composite. Besides, porous silica is a common class of porous materials to enhance the functionality because of their high porosity and surface area. Moreover, porous silica has the advantages of low toxicity, biocompatibility and facile surface functionalization.[57] Mesoporous silica coating can be grown by using cetyltrimethylammonium bromide (CTAB) as surfactant[58] while hollow mesoporous silica coating can be implemented by using a two-step approach, involving the formation of two silica shells and a surface-protected hot water etching process. Liu and co-workers fabricated a yolk nanostructure with mesoporous SiO_2 shell.[59] They obtained different cavity sizes by modifying the etching durations. Apart from combining with other materials, nanoporous composite can be fabricated by novel techniques. Cheng *et al*. recently reported on the fabrication of porous aerogel monolith consisted of Eu

and Tb-doped Y_2O_3 nanosheet. [60] They showed that such porous structure can be fabricated by a simple centrifugation-induced gelation method, followed by supercritical drying in CO_2. The porous structure can readily accommodate gold NPs (AuNPs) for multifunctional applications. Figure 6 (c) shows the as-fabricated porous nanocompsite with AuNPs. The red color is the inherent color of AuNPs due to plasmonic absorption. Another study suggested that polymethylmethacrylate (PMMA) could be used as a template to form marcoporous structure by sol-gel method. [61] The as-prepared composite possesses a periodic luminescent structure, which allows modulation of luminescence.

3.4. Surface modification and functionalization

Surface functionalization and modification techniques are essential to conjugate other materials with luminescent materials for multifunctionalities, particularly in biomedicine application. Note that core-shell growth, silanization, combining with organic small molecules (*e.g.* fluorescent dyes and chemodosimeter molecules) and other surface modification techniques had been reviewed in many review articles. We omit the detailed description in this article and interested readers may find the relative information for fabricating the nanocomposites in the previously published review.[62]

4. Multifunctional applications

In recent years, there is a growing trend to apply luminescent materials to advanced materials and the synthesized composites have been demonstrated to be very promising in multifunctional applications, ranging from optoelectronic to biomedical areas. The purpose of this section is to briefly describe some research examples in these areas and to anticipate that more exciting results will be produced along this direction in the near future.

4.1. Optoelectronics and photonics

This part will review the novel applications of luminescent ions in composites for optoelectronic and photonics devices. Luminescent composites possess multifunctional optical and electrical properties, which are very attractive for fabricating devices to meet the increasing needs in optoelectronic and photonics applications, including light emitting diodes (LEDs), photodetector, waveguide, and novel display.[63] The selected application samples are listed as follows.

4.1.1. Electroluminescence device

It is well-known that various kinds of EL are fundamental to display and solid-state lighting. Recently, EL devices made from the luminescent ions doped phosphors have been developed. From ZnS:Cu in PDMS, highly stretchable and self-deformable alternating current EL devices have been fabricated.[64] Our group has demonstrated a flexible EL device based on a polymer-phosphor composite. [65] The structure of flexible EL device is composed of a single- layer graphene as a top electrode and an optical transparent polyethylene terephthalate (PET) substrate. The as-prepared flexible polymer composite containing metal ion-doped ZnS (ZnS:Al,Cu,Mn) and PDMS was used as the phosphor layer, and an Au thin film on PET was employed as the bottom electrode. Conventionally, indium tin oxide (ITO) film is commonly utilized as a transparent conductive electrode. However, the brittle property of ITO hampers its bending in flexible optoelectronic devices. Differing from ITO film, the large-area chemical vapor deposition (CVD)-grown graphene used here owns good flexibility, excellent mechanical properties, high optical transmittance, and electrical conductivity. The configuration of the flexible EL device is simpler than that of traditional alternate current electroluminescence (ACEL) rigid device where inorganic dielectric layer is usually needed. When an alternating voltage of 100 V at the frequency of 1 kHz is applied to the EL device, white light-emission was detected. **Figure 7** (a) displays the EL spectrum of the device. The inset photograph presents the bright white light-emission which can be observed by the naked eyes, even though the flexible device was greatly bent. Note that the white EL spectrum

includes two main peaks of 512 nm and 588 nm, plus one minor shoulder band located at around 460 nm. The emission bands originate from the corresponding energy transitions of luminescent ions. Obviously, further works are needed to reduce threshold voltage and increase luminous efficacy of the devices.

4.1.2. Optical limiting

With the development and application of high power laser sources, efficient optical limiting materials are increasingly needed to protect human eyes and numerous delicate photonic devices. Optical limiter should have high transmittance for low-input optical intensity while blocking the intense laser beam. Till now, both organic and inorganic optical limiting materials have been studied. Among them, graphene consisted of sp^2-hybridized carbon atoms with 2D structure has shown unique optical, and mechanical properties. Meanwhile, optical limiting performances of graphene-based materials can be enhanced through functionalized with organic molecules or inorganic nanomaterials via covalent bonding. Considering the long lifetime (~ ms) of Ln ions in $NaYF_4$ nanocrystals under NIR laser excitation, it is highly feasible to combine GO with upconversion NPs to develop a novel nanocomposite working in a broadened channel for optical limiting. GO functionalized with luminescent NPs was fabricated by *in situ* growth of $NaYF_4$:Yb^{3+}/Er^{3+} NPs.[51] Figure 7 (b) presents the optical limiting curves of $NaYF_4$:Yb^{3+}/Er^{3+}, GO, and GO/$NaYF_4$:Yb^{3+}/Er^{3+} (GO-Er) excited under 800 nm femtosecond laser, with 70% linear transmittance of all the solutions. Apparently, both GO and GO-Er display super optical limiting behavior. With an increase in high input power, the output powers are held at 137 and 48 mW for GO and GO-Er, respectively. The optical limiting threshold was determined to be 380 and 134 mW for GO and GO-Er, respectively. This result means that GO-Er possesses much better optical limiting effect than GO. The observations are interpreted as the reasons, including nonlinear scattering, nonlinear refraction, and nonlinear absorptions, including free-carrier absorption, two-photon absorption, consecutive two-quantum absorption by impurities/dopants, and reverse saturable absorption.

4.1.3. Optical waveguide

Optical waveguide amplifiers are fundamental devices for the optical communications technology. In particular, Er-doped waveguide amplifiers (EDWAs) are dominating products in this field. Because NIR emission of the Er^{3+} ion at around 1550 nm is the best choice suiting for long distance communications in low loss silica fibers. Note that the utilization of polymeric matrix for the fabrication of optical waveguide amplifiers provides more benefits, such as simplified processing steps, low fabrication costs, and compatibility with patterning techniques. Polymer composite optical waveguides dispersed by Yb-Er nanocrystals were examined. The recorded optical gain at 1.53 μm confirmed the promising waveguide amplifiers. [66] Molard *et al*. fabricated Er^{3+} doped Mo_6-PMMA hybrid copolymer pellets through bulk copolymerizing method.[67] As shown in Figure 7 (c), the prepared composite polymers are optically transparent, suggesting the absence of macroscopic segregation of the inorganic moieties in the organic hosts. Under UV light, Er^{3+} doped Mo_6-PMMA composites present red luminescence. More importantly, Er^{3+} doped Mo_6-PMMA composites show efficient emission at 1530 nm, which originates from Er^{3+}:$^4I_{15/2}$ $^4F_{7/2}$ transition. The results suggest that the fabricated composite can be potentially applied in optical amplifiers. Based on the upconversion luminescent $NaYF_4$ NPs, arrayed waveguide gratings on the luminescent layers were fabricated. As shown in Figure 7 (d), the prepared devices allow for fabricating transparent upconversion displays operated in nonprojection mode by pumping patterned upconversion luminescent composite layers on the cross-point of the waveguides with two NIR lights at 850 and 1500 nm through *X*-axis and *Y*-axis waveguides, respectively. [68]

4.1.4. Novel display

Developing luminescent materials with tunable emission colours is of great significance for novel colour display technologies. More recently, Liu's group in Singapore found that dynamically fine-tuning emission in the full colour range can be achieved by adjusting the pulse width of infrared laser beams.[69] This work represents an exciting advance in tuning

luminescence since it greatly differs from traditional chemical route, i.e. changing composition of the phosphors. As shown in **Figure 8** (a), when pumped by an 808 nm c.w. laser, the blue emission at 470 nm is generated as a result of energy transfer from the core to the first shell by Nd^{3+} Yb^{3+} Tm^{3+}:$^1G_4$. Interestingly, the colour-tunable emission from Ho^{3+} can be realized under 980 nm excitation with changed pulse widths. A non-steady-state upconversion process take responsibility for colour-tunable Ho^{3+} emission, in which deactivation of the excitation energy and the energy transfer process do not happen at the same rate. Because the population of excited states at a specific energy level demands successive pumping of its lower-lying energy levels, radiative transitions from different energy levels may occur at different time intervals. In the view of application, the experiment provides an opportunity of employing the both multiprimary temporal and spatial colour combination demanded for full-colour volumetric three-dimensional displays. In their experiment, the prepared luminescent nanocrystals were incorporated into a PDMS monolith to create a transparent display matrix. Owing to the nonlinear nature of signal generation in photon upconversion, only nanocrystals within the focal volume of the laser beam can be excited. By accompanying the 808 nm c.w. laser with a pulse-modulated 980 nm beam, a novel three-dimensional image can be produced by moving the focal point of the beam within the volume of the display matrix. As shown in Figure 8 (b), luminescence colour images generated in the nanocrystal/PDMS composite monolith show the ability to display three-dimensional objects with wide colour gamuts using the as-developed display system.

Apart from the above lanthanide doped composite, TM ions doped ZnS was also utilized in novel display system. Based on flexible luminescent composite of metal ions doped ZnS microparticles and PDMS matrix, a novel display system with mechanoluminescence (ML) is illustrated by Jeong *et al*. in Korea.[45] When applying pressures, piezoelectric polarization charges are generated within piezoelectric ZnS. The potential originated from the piezo-charges effectively tilts the band structure and consequently facilitates the detrapping of

electrons into the conduction band of metal ions doped ZnS. The energy produced by recombination between detrapped electrons and holes can be transferred to the luminescent ions. Finally the emissions are produced from energy transitions of the materials. The emission color of the polymer composites can be modulated by tuning the mixing ratio of different ions doped ZnS particles (*e.g.*, green for ZnS:Cu; orange for ZnS:Cu,Mn) and specific stimuli conditions (*e.g.*, vibration frequency). As shown in Figure 8 (c), using the patterned ML composite, a new type of harnessing wind-activated display is presented. [70]

4.2. Energy and photocatalysis

Searching renewable and sustainable energy is highly desirable for solving the crucial problems of energy shortage and environmental pollution. In this regard, solar cells and photocatalysis may provide a solution owing to their potential in solar energy conversion. An effective utilization of solar energy had long been attempted through an approach of spectral conversion. In particular, proper spectral manipulation can be employed via mixing luminescent ions into composites for better solar light harvesting.[71]

4.2.1. Solar cell

Dye-sensitized solar cells (DSSCs) have been regarded as one of third generation of photovoltaic devices in the solar energy conversion sector, owing to their transparent configuration, relatively high performance and low fabrication cost.[72] In DSSCs, dyes as sensitizers are usually attached to the surfaces of a semiconductor (typically TiO_2) film to assist sunlight absorption. After light absorption, the electronically excited dye will inject electrons into the conduction band of the film. Considering this, the efficiency of the DSSCs to a great extent is determined by the sensitizer. However, the light absorption edge in the most frequently used Ru-based dyes (*e.g.*, N3 and its derivatives) is limited to ~700 nm due to their optical bandgap (~1.8 eV). Hence, harvesting of the infrared region of sunlight is desirable for sensitizers to improve the device's performance. Previous work on DSSC reports

that Yb^{3+} and Er^{3+} ions as upconversion converters were doped into the TiO_2 hollow sphere by a sol-gel process (**Figure 9** (a)).[73] The system under simulated solar light irradiation yields a maximum quantum efficiency (QE) of 9.12%, which marked a 32.7% improvement as compared to the pristine P25 photoanode (Figure 9 (b)). The enhancement in short-circuit current density (J_{sc}) can be reasonably considered as a result of the upconversion effect of the NPs-TiO_2 composite. Photons around 980 nm are absorbed by Yb^{3+} ions, and then the energy transfer is occurred from Yb^{3+} to Er^{3+} ions. The excited Er^{3+} ions generate green and red upconversion emission bands placed around 533/547 nm and 658 nm, respectively. These bands can be ascribed to the radiative transitions of Er^{3+}:$^4S_{3/2}/^2H_{11/2}$ $^4I_{5/2}$ and $^4F_{9/2}$ $^4I_{15/2}$, respectively. Finally, the light harvesting efficiency will get enhanced since the NIR light is converted *in situ* to the dye-absorbable visible light. The challenge within this cell is that the typical red upconversion emission originating from the transitions of Er^{3+}:$^4F_{9/2}$ $^2I_{15/2}$ at 650 nm cannot be absorbed by the dye in the system. This issue might be incompletely addressed through the employment of dye molecules with an absorption at the red emission range. As presented in Figure 9 (c), Luoshan *et al*. used */3*-$NaYF_4$:Er^{3+}/Yb^{3+} (NYFYE) and graphene multi-functional composite layer as photoanodes in a DSSC.[74] Graphene doping here can improve the dye absorbed. Accordingly, NYFYE@SiO_2 composite enhanced light scattering and NIR light upconversion harvesting. Finally, J_{sc} got apparently enhanced, as displayed in Figure 9 (d).

4.2.2. Photocatalysis

As aforementioned, TiO_2 is widely used compound due to its fascinating characteristics, such as abundance, chemical stability, environmentally friendly, high oxidative power and low cost. However, TiO_2 has a wide band gap of 3.0-3.2 eV and needs to be excited by UV light, which only occupies 5% of solar light. Besides the UV region, the residual 45% and 50% of solar light are comprised by visible light and NIR light, respectively. The limitation of intrinsic properties of TiO_2 renders it photocatalytic applications for the removal of organic

and inorganic pollutants, hydrogen generation, as well as in DSSCs. Hence, there is still a plenty room for TiO_2 to be enhanced for photocatalysis using solar light. To address this issue, some strategies, such as heterostructure, dye sensitizing, and luminescent ions doping have been proposed. For example, (Yb,Er)-$NaYF_4$/C-TiO_2 composite was considered so that not only UV but also weak visible and NIR lights are effectively stimulated, due to the improved carbon doping concentrations and photon energy transfer between upconversion phosphor and carbon doped TiO_2.[75] Under the irradiation of UV, visible and NIR lights, the photocatalytic performances of as-prepared samples were studied by recording the NO_x gas destruction ability. **Figure 10** (a) presents the deNO_x activity of several samples utilizing varied wavelengths of light sources and all the samples were reserved in dark for 30 min before irradiation to reduce the impact of absorption of NO species by samples. For (Yb,Er)-$NaYF_4$, there was no obvious deNO_x activity regardless of irradiation wavelengths. As for pure C-TiO_2, 0%, 6.2%, 23.2%, 28.3% and 32.9% of NO were decomposed under the excitation of NIR diode laser, red, green, blue and UV LED, respectively. The good visible light stimulated photocatalytic activity for this sample was mainly ascribed to the excellent absorption of C-TiO_2, while no NIR light driven deNO_x activity was achieved, and pure C-TiO_2 could not be excited by NIR light. However, when combining C-TiO_2 photocatalyst with (Yb,Er)-$NaYF_4$ upconversion phosphor, about 8.5% of NO_x gas was successfully obtained even when using a NIR diode. This NIR light stimulated activity could be ascribed to the synergetic effect of C-TiO_2 photocatalyst and (Yb,Er)-$NaYF_4$ upconversion phosphor. In addition, the deNO_x ability of (Yb,Er)-$NaYF_4$/C-TiO_2 was also studied by using NIR laser, red LED, both NIR laser and red LED as irradiation sources (Figure 10 (b)). It was clearly shown that about 19% of NO_x gas was destructed under red LED. While further 4.5% of NO_x gas reduction was appeared when NIR laser was combined with red LED as the light source. This result suggests that the (Yb,Er)-$NaYF_4$/C-TiO_2 composite can simultaneously present the outstanding continuous NO_x gas destruction ability under the irradiation of UV, visible and NIR lights.

In addition, plasmonic Au NP decorated $NaYF_4$:Yb^{3+},Er^{3+},Tm^{3+}-core@porous-TiO_2-shell composite was fabricated as photocatalysis.[76] The designed structure could favor the efficient charge or energy transfer among constituent nanocomponents due to plasmon and upconversion effects. The prepared composite exhibits good stability, high surface area, broadband absorption from UV to NIR, and excellent photocatalytic activity, considerably better than the benchmark P25-TiO_2. Figure 10 (c) shows the mechanism for NIR-driven photocatalysis of the prepared composite. First, Yb^{3+} ions absorb the 980 nm illumination due to a large absorption cross section, leading to the population of the $^2F_{5/2}$ level in Yb^{3+}. After that, the efficient energy transfers from Yb^{3+} to Tm^{3+} and Er^{3+} ions, resulting in the excited Tm^{3+} and Er^{3+}. Then the transitions of $^1I_6$ $^3F_4$, $^1D_2$ $^3H_6$, $^1D_2$ $^3F_4$, and $^1G_4$ $^3H_6$ of Tm^{3+} generate UV and blue emissions, centered at 345, 361, 451, and 477 nm, respectively. For the green emission peaked at 521 and 540 nm, which covers the surface plasmon resonance band of the Au NPs, are originated from the transitions of $^2H_{11/2}$ $^4I_{15/2}$ and $^4S_{3/2}$ $^4I_{15/2}$ of Er^{3+}, respectively. The upconverted UV emission from the luminescent NPs can be efficiently absorbed by the TiO_2 shell closely surrounding the core, as demonstrated by the experimental and theoretical investigations. Such energy transfer can yield electron/hole pairs in the TiO_2, same as under UV irradiation, which can consequently contribute to catalytic reactions. Simultaneously, the upconverted green emission from the luminescent ions can be absorbed by neighboring Au NPs to excite their surface plasmon resonance. Then photo-induced hot electrons from the Au NPs are transferred to the CB of TiO_2. Consequently, both the energy transfer to close TiO_2 and Au NPs from the luminescent ions assists to progress the NIR photocatalytic activity.

4.3. Biomedicine

This part will review the novel applications of luminescent composites in the biological field. Although the low luminescence of near infrared-triggered upconversion (UC), very

recent work indicated that dye-sensitized core-shell structure can improve the luminescence efficiency.[77] Moreover, luminescent nanocomposites possess multifunctional physical and chemical properties, which are important for building the platform to meet the increasing needs in biological applications, including multimodal bioimaging, biosensing, drug delivery and therapies.

4.3.1. Multimodal bioimaging

Bioimaging is a useful bio-diagnostic tool for visualization of internal organs and functional information. The development of multimodal bioimaging is of prime importance because the synergetic effect of different modes can compensate the weakness of specific modes.[78] The physical properties of luminescent ions, especially Ln ions, possess additional properties, for example, the series of Ln ions can absorb X-ray and gadolinium ion presents magnetism. [3] These properties contribute to the multimodality for biological diagnostics at different depths. So far, bi- or tri-modal upconversion luminescence (UCL)/X-ray or X-ray computed tomography (CT)/magnetic resonance imaging (MRI) are reported by various groups. [79] The emission from Ln-doped nanoparticles played important role in the optical imaging depth. It is desirable that the emission from such nanoparticles fall into the NIR-I and NIR-II window, because the scattering effect of visible light in biological tissue greatly limit the imaging depth.[78]b There are a few Ln ions that possess emissions in the NIR regime, for example Yb^{3+}, Nd^{3+}, Tm^{3+} and Er^{3+} ions (Table 1). The imaging depths of these ions can be extended up to 2 mm *in vivo*.[78]c Despite their respective strength, these imaging modes still suffer from some drawbacks, such as ionizing radiation and poor resolution. The development of luminescent nanocomposites can overcome such problems. The combination of luminescent materials with radioactive isotopes enables positron emission tomography (PET) and single photon emission computed tomography (SPECT). Li's group in China has done influential works on multimodal bioimaging. They fabricated nanocomposite comprising $Gd^{3+}/Yb^{3+}/Er^{3+}$ doped $NaYF_4$ and radioactive fluorine-18 isotopes for multimodal

PET/MRI/UCL bioimaging. [80] In addition to MRI/UCL imaging, PET imaging expanded the study of the injected imaging probe from cellular to whole body. The biodistribution of the nanocomposite can be visualized by using PET imaging. In a later work, radioactive ^{153}Sm was doped into the shell of core-shell $NaLuF_4$:Yb/Tm@$NaGdF_4$ as nanocomposite for four modal SPECT/MRI/X-ray/UCL bioimaging. [81] SPECT imaging can provide not only biodistribution information, but also absolute quantification of imaging ability. Importantly, the synergetic effect of the four imaging modes was demonstrated in the tumor angiogenesis analysis and proved the high potential of clinical application of the nanocomposite. Besides, it is worthwhile to note that the successful integration of photoacoustic (PA) imaging into luminescent nanocomposites has provided new opportunities for the researches in multimodal bioimaging because PA is an emerging clinical technique combining the merits of optical and acoustic imaging. This technique displays good planar resolution and large imaging depth. Maji *et al*. presented their work on using UCNPs for PA imaging. [82] Their results demonstrated combining UCNPs with inclusion complex *a*-cyclodextrin. The nanocomposite can be excited by 980 nm excitation to give UCL and PA signal simultaneously. However, the number of modalities in a single material should be as large as possible because it can avoid injection of multiple contrast agents. Recently, Rieffel *et al*. developed a hexamodal bioimaging system by using porphyrinphospholipid (PoP)-coated upconversion nanoparticles. [83] **Figure 11** shows the six imaging modes, including fluorescence (FL), UCL, PET and CT, Cerenkov luminescence (CL) and PA imagings after the injection of the nanocomposite for 1 h at the lymph node, all of the imaging modes suggested the accumulation of the nanocomposite in the lymph node. Despite the excellent imaging quality and various imaging modes in the material system, further assessment of *in vivo* toxicity is needed to conclude the biosafety of this nanocomposite for potential clinical application.

4.3.2. Biodetection

In addition to multimodal bioimaging, luminescent nanocomposites may also contribute to the field of biodetection. Nowadays, there are many developed proof-of-concept biodetection readout systems; optical system is one of the ideal choices mainly because of its high sensitive. [84] There are mainly two types of luminescent biodetection systems divided into homogeneous and heterogeneous system. [85] The former is a type of assay performs in liquid phase while the latter is in solid phase. Recently, we reported a novel heterogeneous assay design by using $BaGdF_5$:Yb/Er UCNPs-anodized alumina nanoporous membrane (NAAO) for Ebola virus oligo detection. [53] The UCNPs are anchored in the hollow channel of the NAAO substrate for detection of Ebola virus oligo. Then, the AuNPs with Ebola virus oligo are in proximity with the UCNPs, which manifested luminescence resonance energy transfer (LRET) for detection. Importantly, the design showed improved limit of detection (LOD) from picomolar (pM) to femtomolar (fM) level (**Figure 12** (a)). Moreover, we demonstrated that the NAAO-based luminescent platform can be used to detect clinical samples of Ebola virus RNA with extremely high sensitivity down to fM level (Figure 12 (b)). Apart from the reported Ebola clinical sample detection, our heterogeneous design may be regarded as a general approach based on upconversion luminescence nanocomposites, opening a new possibility for detecting various types of viruses. In addition to NAAO, the use of paper as template for biodetection could effectively reduce the cost and increase the robustness of luminescent biosensors in nature. Very recently, Song's group presented a paper-based upconversion LRET biodetection platform for carcinoembryonic antigen (CEA). [86] The structure of the paper device is presented in Figure 12 (c). The area of the detection platform and droplet of UCNPs were firstly confined by printing hydrophobic copper sulphate nanoparticles on a filter paper. In their platform, UCNPs and FITC were used as the energy donor and acceptor, respectively. By utilizing the antibody-antigen interaction, the UCNPs and FITC are in proximity and the upconversion luminescence was effectively absorbed by FITC, yielding a LOD of 0.89 ng/ml. Furthermore, multi-channel paper device was fabricated

for simultaneous detection of three types of mixed cancer biomarker by the same method (Figure 12 (d)). As a result, this paper device appeals to clinical point-of-care detection for cancer markers. Apart from the aforementioned biodetection systems, more advanced biodetection can be carried out in living cells or even mouse models. For example, Zhang's group demonstrated that the use of UCNPs-SiO_2 core shell structure for intra-cellular DNA detection.[87] The DNA loaded UCNPs acted as cargo to deliver the gene into the cell cytoplasm, in which the DNA release can be monitored by LRET. Apart from DNA release, UC-based LRET can also be used for the detection of hypochlorous acid (HOCl).[88] The UCNPs were modified with RBH1 via hydrophobic interaction to form a nanocomposite. The intracellular studies suggested that HOCl can be detected by a ratiometric UCL method. The detection of heavy metal ions are of great importance because of the cytotoxic and accumulation effects of such ions. Li's group reported a sensitive UCNPs-cyanine dye system for the detection of methylmercury ions ($MeHg^+$).[89] Interestingly, the interaction of the probe and the target $MeHg^+$ led to the increase in red and decrease in near infrared emission. The two wavelengths both yield high LOD. To further validate the *in vivo* detection ability, the $MeHg^+$ was injected intravenously into Kunming mice. The results indicated that the system worked well at both in *vivo* and *ex vivo* conditions.

4.3.3. Drug delivery and phototherapy

Despite the development of sensitive biodetection schemes, drugs are required to cure the diseased sites. A carefully designed drug delivery system should be able to prevent possible digestion, absorption or degradation of the drug by organs before reaching the diseased site. [90] As a result, luminescent nanocomposites should be an option to face the challenge. Doxorubicin (DOX) has been routinely used as a drug model for many proof-of-concept anti-tumor drug delivery systems. [91] Lin's group has done man e cellent or s along this direction. They fabricated a multifunctional upconversion nanocomposite with smart polymer brushes gated mesopores for thermo/pH dual-responsive drug controlled release and

bioimaging application. [57c] The dual responsive mechanism is stemmed from the poly[(N-isopropylacrylamide)-co-(methacrylic acid)] copolymer. Firstly, the brushes can be opened at low pH value because of high acidity at tumor sites. Then, the low critical solution temperature characteristic of the copolymer allows the system to release the loaded DOX upon increased temperature due to the shrinkage of the polymer brushes. Moreover, they showed that the release rate of the DOX can be enhanced by using NIR radiation because 980 nm laser excitation posed heating effect to water. As a result, the drug release rate can be further increased up to 9.55 % in 40 min. Careful spectral designs may also benefit to photo-triggered drug release systems. Yang *et al.* designed a photo responsive drug release system by using UCNPs with mesoporous shell.[92] DOX is firstly conjugated to the shell via a UV cleavable theo-nitrobenzyl (NB) caged linker. The NB linkage is cleaved upon UV emission from the UCNPs. The conjugation of folic acid on the system further enhances the antitumor ability as evidenced in the HeLa and NIH/3T3 cell lines. The use of photoactivatable prodrug can be another approach to design photo-triggered drug release systems. Dai *et al.* conjugated the trans-platinum (IV) pro-drug to UV emitting UCNPs for near infrared triggered drug release.[93] It is important to highlight the use of prodrug can reduce the cytotoxicity due to leakage during delivery to disease site. Therefore, this drug release system not only possess the inherent merits of photo responsive drug release but also able to reduce the unwanted side effects. In addition to upconversion luminescence (UCL), long persistence luminescence nanophosphors (LPNP) are drawing increasing attention in biological application owing to their unique luminescent property. [94] In fact, such persisting luminescence may be useful for prolong biological experiments, such as cell tracking, cell growth and drug release monitoring. It is reported the mesoporous silica-coated long persistence phosphors could be used for drug delivery and tumor imaging. [95] The afterglow of the folic acid (FA) modified-$Zn_{1.1}Ga_{1.8}Ge_{0.1}O_4:Cr^{3+}$, Eu^{3+} @SiO_2 LPNPs showed duration up to 15 days after ultraviolet excitation followed by red light emitting diode (LED). The DOX was loaded in the

mesoporous silica shell and then the LPNPs were subsequently injected into the mouse via intravenous injection. **Figure 13** (a) shows the *in-vivo* and *in-situ* monitoring of DOX in the H22-tumor bearing mouse. Owing to the targeting ability of FA, the afterglow signal can be detected at the tumor site as indicated by the yellow arrow. Figure 13 (b) is the corresponding image after secondary excitation by using red LED for 2 min. Their study indicated that long persistence phosphors are potential candidate for trackable drug delivery.

In addition to drug delivery application, nanocomposites are attractive class of material for phototherapies. Photodynamic therapy (PDT) and photothermal therapy (PTT) are the two commonly used types of phototherapies. The former requires photon sensitizer to produce oxygen singlets ($^1O_2$) to kill tumors[96] while the latter involves the production of heat by the photon sensitizer to kill tumors by extensive heating effect.[97] However, it should be noted that NIR-triggered phototherapies offer larger penetration depth than UV/visible light excited ones. [98] Idris *et al*. developed a hybrid system composed of $NaYF_4$ UCNPs and two photon sensitizers, merocyanine 540 (MC540) and zinc (II) phthalocyanine (ZnPc) for improved PDT. [99] $^1O_2$ was produced efficiently owing to the good spectral overlapping of the UCL and absorption spectra of MC540 and ZnPc. Moreover, the tumor suppression effect was assessed by monitoring the tumor volumes of the different treatment group of mice over a period of two weeks. Figure 13 (c) indicates the differences in the tumor size of different testing groups before and after PDT treatment. It is clear that the nanocomposite with FA and polyethylene glycol (PEG) surface modification (group 1) demonstrates better PDT effect than that with no modification (group 2) because of tumor targeting effect. Similar findings were presented by other researchers on the use of $NaYF_4$-ZnPC for *in vivo* PDT applications. [100] In this experiment, ZnPC is the key element for production of $^1O_2$ and they found that the nanocomposite can achieve PDT for 1 cm depth tumors. On the other hand, gold nanoshells and nanorods are well-documented examples for PTT because of their ability to produce heat under illumination of NIR excitation. [101] By layer-by-layer growth method, Cheng *et al.*

developed core-shell-shell multifunctional nanoparticles (MFNPs) consisted of a $NaYF_4$:Yb/Er core/iron oxide shell/gold nanoshell structure. [102] Unlike other reported PTT work, this nanocomposite can perform magnetically-guided PTT effect under magnetic field. Figure 13 (d) presents the 4T1 tumor bearing mice in different testing groups. It is obvious that the mouse with injected MFNPs showed substantial tumor shrinkage under magnetic guidance and laser illumination for PTT. They also observed no tumor re-growth over 40 days. In addition, $NaYF_4$:Yb^{3+},Er^{3+}@Ag core/shell nanocomposites were fabricated for UCL imaging and PTT application. [103] The silver shell can not only provide heating effect for PTT, but also reduce the toxicity. It is apparent that PDT and PTT are two powerful tools for tumor suppression. As a result, the combination of the two phototherapeutic techniques can further enhance their abilities in theranostics. It is showed that the two techniques can be synergistically combined in their obtained core-shell UCNPs-nanographene oxide/ZnPC composite. [104] The 808 nm laser excitation is absorbed for bioimaging and PTT application while the PDT is triggered by illumination of 630 nm laser. Compared to PDT and PTT alone, the integration of PDT and PTT can enhance the efficacy towards cancer therapy.

4.4. Sensors

Recently, novel fluorescent sensors based luminescent ions have been demonstrated, particularly utilizing the stimuli responsive properties of luminescent composites. In principle, fluorescent sensors can provide the output luminescence performances with a high spatial resolution, non-destructive, and real-time modes. In this part, selected luminescent sensors based luminescent ions doped composites will be introduced.

4.4.1. Stress sensor

Stress-sensing materials with high spatial resolution enable one to monitor structural health and impending failure through the dispersion of nano-sensor particles when used as surface coatings or adhesives on load-bearing structures. Raghavan *et al*. embedded photoluminescent

Cr^{3+} doped *a*-alumina nanoparticles into a polymer matrix to monitor the stress distribution within the composite material in an *in situ* configuration. [105] Their idea is shown in **Figure 14** (a) and (b). An adhesive and fiberglass substrates were used in this single lap-shear experiment. The integrity monitoring technique can be utilized to predict the eventual and weakening failure of a bonded joint by relating obtained quantitative stress measurements from PL with the stress evolution of the composite (Figure 14 (c)). This nondestructive technique with piezospectroscopy records stress-induced shifts of the photostimulated emission lines of Cr^{3+} doped *a*-alumina during laser excitation. These characteristic R-emission lines are originated from optical transitions between excited states and the ground state of Cr^{3+} ions within *a*-alumina. One of the most important features for this approach is the presence of high spatial resolution, because the excitation laser beam can be focused on the composite with an optical microscope or fiber optic probe. The quantum efficiency of Cr^{3+} luminescence is very high so that an abundant emission signal can be measured from the polymer composite. Therefore, this luminescent composite sensing system will enable quantitative measurement and non-invasive monitoring of stress distributions applied as adhesives or as coatings on a substrate under loading conditions.

Electronic signature for identity verifications is necessary to collect more-personalized information during signing, with an extensive promising applicability in human-machine interfaces and artificial intelligence. It is desirable to make highly sensitive, large-size, fast-response, and high-spatial-resolution pressure sensor arrays. Recently, Wang and Pan's group made a breakthrough to develop a new dynamic pressure mapping of personalized handwriting by a flexible composite sensor based on the ML process. [106] They developed the pressure sensor through mixing ZnS:Mn microparticles with positive photoresist. Therefore, this pressure sensor based on the ML composite can record pressure mapping using self-generated light emission. Figure 14 (d) presents dynamic pressure visualization by capturing a handwritten letter 'e' in real-time. The corresponding gray scale of the real-time captured

image based on the ML intensity can be used to record both handwritten signatures and the signing habits of a few signees (Figure 14 (e)).

4.4.2. Thermometer

Traditional liquid-filled and bimetallic thermometers are normally not appropriate for temperature quantities at scales belo 10 μm. Therefore, it demands developing new non-contact accurate thermometers with high spatial resolution. Fortunately, the temperature dependence of metal-ion-doped phosphor luminescence is a non-invasive and accurate alternative method that operates remotely by way of an optical detection system, even in fast-moving objects, strong electromagnetic fields, and biological fluids. [107] For instance, Carlos *et al*. developed a luminescent nanothermometer based on Eu^{3+}/Tb^{3+} doped NPs. [108] The nanothermometer consisted of Eu,Tb codoped y-Fe_2O_3@TEOS/APTES nanocomposites. Under the excitation, the intensity of the green Tb^{3+} luminescence obviously shrinkages as the temperature rises, whereas the intensity of the red Eu^{3+} lines starts to rise at precisely the same temperature at which the Tb^{3+} emission for NP3-1.3 (1.3 means Eu:Tb=1:3) starts to decline. Figure 14 (f) shows the temperature dependence of the Commission Internacionale d'Eclairage (CIE) (,) color coordinates of the composites. Apparentl , the composite thermometer presents variable color depending on temperature, due to different energy levels in Tb^{3+} and Eu^{3+} ions. The Tb^{3+} ions own an excited triplet state with energy slightly above that of $^5D_4$ emitting state, thus warranting the occurrence of thermally-driven $^5D_4$ host energy transfer. Therefore, the Tb^{3+}: $^5D_4$ emission is temperature dependent. Whereas the energy difference between that triplet state and the Eu^{3+}: $^5D_0$ excited level is too large to permit thermally-driven depopulation, the Tb^{3+}/Eu^{3+} relative intensity warranties the absolute quantity of temperature. Meanwhile, the spatial resolution of the thermometer can be varied by tuning the size of the luminescent nanocomposites. Besides Eu^{3+}/Tb^{3+} codoped NPs for temperature sensing, other Ln^{3+} doped NPs such as Er^{3+}/Yb^{3+} codoped NPs[109] and Nd^{3+}/Yb^{3+} codoped materials[110] also have outstanding temperature responsive properties.

4.4.3. Magnetic sensor

Compared to the PL and EL as aforementioned, little work is reported on the light emission by another common source, *i.e.* magnetic field. The correlation between light emission and magnetic field stimulation has often been ignored. Very recently, our group has developed a magnetic-induced luminescence (MIL) device based on flexible composite laminates, by coupling the magnetic field to piezo-phototronic process.[111] We fabricated multiphase rods consisted of the luminescent composite of metal-ion-doped ZnS microparticles mixed to PDMS and another magnetic composite of Fe-Co-Ni alloy particles mixed to PDMS. When applying magnetic fields with varied frequency *f*, the luminescence spectra of ZnS:Al,Cu phosphors combined with Fe-Co-Ni+PDMS are presented in Figure 14 (g). The main peak is observed at 509 nm, which can be ascribed to the donor-acceptor (D-A) recombination of Al_{Zn}–Cu_{Zn} as displayed in the inset of Figure 14 (g). MIL originates from synergistic effect between magnetic field and piezophotonic process. Under magnetic fields, the strain produced by the magnetic elastomer trigger an inner piezoelectric potential in the metal-ion-doped ZnS particles. And then the luminescence is generated within the composite without need of using a power unit. Importantly, we demonstrated the linear relationship of MIL intensity versus *f* and H_{rms}^{2}, as presented in Figure 14 (h). The inset in Figure 14 (h) displays photograph of displaing green colored logo "PU" from MIL materials driven by low magnetic field. The good linear relationship between the input and output signals, and self-generated light suggest that this luminescent composite should be benefit to develop novel MIL-based magnetic sensors. In real world, magnetic fields exist in many systems, and therefore the detection of magnetic field is essential for environmental surveillance, mineral exploring, and safety monitoring. In contrast to conventional magnetic sensors employing the conversion from magnetic field input to electric signal output, the MIL based sensors proposed by our group enjoy competitive merits, including real-time visualization, remote sensing without making

electric contact, nondestructive and noninvasive detection. Therefore, this work presents a new opportunity for magnetic materials. [112]

5. Summary and outlook

In this feature article, luminescent ions in advanced composite materials for multifunctional applications have been comprehensively reviewed. Combining two or more phases of different materials into one composite is a complementary strategy for advanced functional materials research. The developed methods allow fabricating or tuning the composite systems with improved or additional properties, which may result in multifunctional applications. For luminescent ions doped phosphors, careful engineering of luminescence profiles attributed to active dopant ions permits the applications of these optical materials in various fields. In fact, those composites by coupling luminescent ions with various types of materials, such as polymers, porous and 2D materials, have generated considerable and widespread interests in many fields, due to their luminescent, superior mechanical, and multifunctional properties. Specifically, luminescent composites with additional optical and electrical properties have been used to fabricate devices to meet the growing needs in novel optoelectronic and photonics applications, such as EL devices, waveguide, optical limiting, novel display and so on. Luminescent ions with upconversion or downconversion in composite materials have been well recognized in making sustainable energy devices for effective solar light harvesting. In biomedicine field, optical techniques based on luminescent ions have recently been exploited for diagnosis, imaging, nanocomposite biosensors, and medical treatment. Apart from the above applications, luminescent ions have also played a significant role in various novel sensors, such as stress, temperature, and magnetic field by luminescence spectra.

Despite encouraging progress on the luminescent ions based advanced composite materials in the past decade, the fast development in nanoscience and biotechnology in the 21st century has aroused increasing number of research into the applications of the new optical composite

materials down to the nanoscale. To follow the research trend, the study of luminescent composites should be further developed. In this connection, surface and interface of the advanced composites are essential to be investigated and modified for optimizing the material's performances. And more types of novel advanced functional materials with the luminescent ions could be designed and fabricated for expanded applications. Hence, there is a plenty room for the applications of luminescent composites in the new forefront of sensor, optoelectronics, solar energy, and biological sciences. For biomedical application, the biosafety of the luminescent nanocomposite should be taken further assessment of *in vivo* toxicity. Optimization of synthesizing luminescent composite materials is a time-consuming task and sometimes it is a technically difficult to carry out. To overcome the obstacles, it demands comprehensive understandings of the fundamental physics and developing related theoretical models, for predicting and interpreting the related synergistic effect in the luminescent composites. For instance, theoretical calculations based on first principles density functional theory (DFT) may be expanded to serve multifunctional luminescent composite systems beyond phosphors for LEDs. [113] In conclusion, advanced composite materials based luminescent ions will become increasingly energetically efficient, miniaturized, sophisticated, reliable, eco-friendly, and low-cost. It is hoped that this feature article will stimulate the research and novel functional materials will play an important role in the cutting-edge technologies.

Acknowledgements

The research was financially supported by the grants from Research Grants Council of Hong Kong (GRF No. PolyU 5005/13P), Innovation and Technology Support Programme (Project No. ITS/057/15), and National Natural Science Foundation of China (Grant No. 11474241).

Received: ((will be filled in by the editorial staff))

Revised: ((will be filled in by the editorial staff))

Published online: ((will be filled in by the editorial staff))

Reference

[1] W. M. Yen , S. Shionoya , H. Yamamoto , *Phosphor Handbook* 2nd ed., CRC Press, Boca Raton, FL **2007**.

[2] G. Bai, M. K. Tsang, J. Hao, *Adv. Opt. Mater.* **2015**, *3*, 431.

[3] M.-K. Tsang, G. Bai, J. Hao, *Chem. Soc. Rev.* **2015**, *44*, 1585-1607.

[4] Y. Zhang, J. H. Hao, *J. Mater. Chem. C* **2013**, *1*, 5607-5618.

[5] J. C. G. Bunzli, S. V. Eliseeva, *Chem. Sci.* **2013**, *4*, 1939-1949.

[6] a) S. Zhou, W. Zheng, Z. Chen, D. Tu, Y. Liu, E. Ma, R. Li, H. Zhu, M. Huang, X. Chen, *Angew. Chem. Int. Edit.* **2014**, *53*, 12498-12502; b) D. Peng, Q. Ju, X. Chen, R. Ma, B. Chen, G. Bai, J. Hao, X. Qiao, X. Fan, F. Wang, *Chem. Mater.* **2015**, *27*, 3115-3120; c) W. J. Jie, J. H. Hao, *Nanoscale* **2014**, *6*, 6346-6362.

[7] C. Larson, B. Peele, S. Li, S. Robinson, M. Totaro, L. Beccai, B. Mazzolai, R. Shepherd, *Science* **2016**, *351*, 1071-1074.

[8] D. M. Yang, P. A. Ma, Z. Y. Hou, Z. Y. Cheng, C. X. Li, J. Lin, *Chem. Soc. Rev.* **2015**, *44*, 1416-1448.

[9] a) L. D. Carlos, R. A. S. Ferreira, V. d. Z. Bermudez, B. Julian-Lopez, P. Escribano, *Chem. Soc. Rev.* **2011**, *40*, 536-549; b) B. Lebeau, P. Innocenzi, *Chem. Soc. Rev.* **2011**, *40*, 886-906.

[10] B. Valeur, M. N. Berberan-Santos, *J. Chem. Educ.* **2011**, *88*, 731-738.

[11] a) Z. L. Wang, J. Hao, H. L. Chan, W. T. Wong, K. L. Wong, *Small* **2012**, *8*, 1863-1868; b) H. T. Wong, H. L. W. Chan, J. H. Hao, *Opt. Express* **2010**, *18*, 6123-6130.

[12] a) P. W. Kuan, K. F. Li, G. Zhang, X. Wang, L. Zhang, G. X. Bai, Y. H. Tsang, L. L. Hu, *Opt. Mater. Express* **2013**, *3*, 723-728; b) Y. Zhang, J. H. Hao, *J. Appl. Phys.* **2013**, *113*, 184112.

[13] a) J. Hao, Y. Zhang, X. Wei, *Angew. Chem. Int. Ed.* **2011**, *50*, 6876; b) G. Bai, L. Tao, K. Li, L. Hu, Y. H. Tsang, *Opt. Mater.* **2013**, *35*, 1247-1250.

[14] a) G. Bai, Y. Guo, Y. Tian, L. Hu, J. Zhang, *Opt. Mater.* **2011**, *33*, 1316-1319; b) G. Bai, L. Tao, K. Li, L. Hu, Y. H. Tsang, *J. Non-Cryst. Solids.* **2013**, *361*, 13-16.

[15] a) H. T. Wong, H. L. W. Chan, J. H. Hao, *Appl. Phys. Lett.* **2009**, *95*; b) Y. S. Liu, D. T. Tu, H. M. Zhu, R. F. Li, W. Q. Luo, X. Y. Chen, *Adv. Mater.* **2010**, *22*, 3266

[16] a) Z. Wu, G. Bai, Q. Hu, D. Guo, C. Sun, L. Ji, M. Lei, L. Li, P. Li, J. Hao, *Appl. Phys. Lett.* **2015**, *106*, 171910; b) H. Lin, T. Yu, G. Bai, M.-K. Tsang, Q. Zhang, J. Hao, *J. Mater. Chem. C* **2016**, *4*, 3396.

[17] a) J. H. Hao, J. Gao, M. Cocivera, *Appl. Phys. Lett.* **2003**, *82*, 2224-2226; b) C. K. Duan, C. C. Ko, G. H. Jia, X. Y. Chen, P. A. Tanner, *Chem. Phys. Lett.* **2011**, *506*, 179-182.

[18] S. Kamimura, H. Yamada, C.-N. Xu, *Appl. Phys. Lett.* **2012**, *101*, 091113.

[19] a) X. S. Wang, C. N. Xu, H. Yamada, K. Nishikubo, X. G. Zheng, *Adv. Mater.* **2005**, *17*, 1254; b) X. Tian, Z. Wu, Y. Jia, J. Chen, R. Zheng, Y. Zhang, H. Luo, *Appl. Phys. Lett.* **2013**, *102*, 042907.

[20] a) I. Nikolov, X. Mateos, F. Guell, J. Massons, V. Nikolov, P. Peshev, F. Diaz, *Opt. Mater.* **2004**, *25*, 53-58; b) M. Grinberg, J. Barzowska, Y. R. Shen, K. L. Bray, B. V. Padlyak, P. P. Buchynskii, *Phys. Rev. B* **2002**, *65*.

[21] a) E. Song, S. Ding, M. Wu, S. Ye, F. Xiao, S. Zhou, Q. Zhang, *Adv. Opt. Mater.* **2014**, *2*, 670-678; b) Z. Lou, J. Hao, *Appl. Phys. A* **2005**, *80*, 151-154.

[22] H. Zhu, C. C. Lin, W. Luo, S. Shu, Z. Liu, Y. Liu, J. Kong, E. Ma, Y. Cao, R.-S. Liu, X. Chen, *Nat. Commun.* **2014**, *5*. 4312.

[23] a) G. X. Bai, Y. Zhang, J. H. Hao, *J. Mater. Chem. C* **2014**, *2*, 4631-4635; b) G. Bai, W. Jie, Z. Yang, J. Hao, *J. Appl. Phys.* **2015**, *118*, 183110.

[24] J. Lin, Q. Su, *Phys. Status Solidi B* **1996**, *196*, 261-267.

[25] a) H.-T. Sun, J. Zhou, J. Qiu, *Prog. Mater. Sci.* **2014**, *64*, 1-72; b) B. B. Xu, S. F. Zhou, D. Z. Tan, Z. L. Hong, J. H. Hao, J. R. Qiu, *J. Appl. Phys.* **2013**, *113*; c) B. B. Xu, G. X. Bai, J. C. Wang, Q. B. Guo, D. Z. Tan, W. B. Chen, X. F. Liu, S. F. Zhou, J. H. Hao, J. R. Qiu, *Opt. Lett.* **2014**, *39*, 3022-3025.

[26] J. Bunzli, S. Comby, A. Chauvin, C. Vandevyver, *J. Rare Earth* **2007**, *25*, 257.

[27] J.-C. G. Bunzli, C. Piguet, *Chem. Soc. Rev.* **2005**, *34*, 1048-1077.

[28] J. F. Jin, Y. J. Gu, C. W. Y. Man, J. P. Cheng, Z. H. Xu, Y. Zhang, H. S. Wang, V. H. Y. Lee, S. H. Cheng, W. T. Wong, *ACS nano* **2011**, *5*, 7838-7847.

[29] C. Zhao, L. Feng, B. Xu, J. Ren, X. Qu, *Chemistry* **2011**, *17*, 7007-7012.

[30] H. Lin, T. Yu, M.-K. Tsang, G. Bai, Q. Zhang, J. Hao, *Appl. Phys. Lett.* **2016**, *108*, 041902.

[31] K. K. -W. Lo, A. W. -T. Choi , W. H. -T. Law , *Dalton Trans.* **2012** , *41* , 6021.

[32] Y. Chi, P.-T. Chou, *Chem. Soc. Rev.* **2010**, *39*, 638.

[33] Y. Zhang, G. Y. Gao, H. L. W. Chan, J. Y. Dai, Y. Wang, J. H. Hao, *Adv. Mater*. **2012**, 24, 1729.

[34] G. Bai, Y. Zhang, J. Hao, *Sci. Rep.* **2014**, *4*, 5724.

[35] M. Y. Sharonov, A. B. Bykov, V. Petricevic, R. R. Alfano, *Opt. Lett.* **2008**, *33*, 2131.

[36] B. B. Xu, J. H. Hao, Q. B. Guo, J. C. Wang, G. X. Bai, B. Fei, S. F. Zhou, J. R. Qiu, *J. Mater. Chem. C* **2014**, *2*, 2482.

[37] W. Feng, C. M. Han, F. Y. Li, *Adv. Mater.* **2013**, *25*, 5287-5303.

[38] S. Yun, S. Park, B. Park, Y. Kim, S. K. Park, S. Nam, K. U. Kyung, *Adv. Mater.* **2014**, *26*, 4474-4480.

[39] S. Kim, J. Byun, S. Choi, D. Kim, T. Kim, S. Chung, Y. Hong, *Adv. Mater.* **2014**, *26*, 3094-3099.

[40] a) M. D. Xiao, H. J. Chen, T. A. Ming, L. Shao, J. F. Wang, *ACS Nano* **2010**, *4*, 6565-6572; b) S. F. Zhou, N. Jiang, B. Zhu, H. C. Yang, S. Ye, G. Lakshminarayana, J. H. Hao, J. R. Qiu, *Adv. Funct. Mater.* **2008**, *18*, 1407-1413.

[41] G. Williams, B. Seger, P. V. Kamat, *ACS nano* **2008**, *2*, 1487-1491.

[42] F. Xia, H. Wang, D. Xiao, M. Dubey, A. Ramasubramaniam, *Nat. Photonics* **2014**, *8*, 899-907.

[43] W. Caseri, *Hybrid Materials*, Wiley-VCH Verlag GmbH & Co. KGaA, **2007**, 49-86.

[44] Q. Guo, R. Ghadiri, T. Weigel, A. Aumann, E. L. Gurevich, C. Esen, O. Medenbach, W. Cheng, B. Chichkov, A. Ostendorf, *Polymers* **2014**, *6*, 2037-2050.

[45] S. M. Jeong, S. Song, S. K. Lee, N. Y. Ha, *Adv. Mater.* **2013**, *25*, 6194-6200.

[46] K.-L. Lei, C.-F. Chow, K.-C. Tsang, E. N. Lei, V. Roy, M. H. Lam, C. S. Lee, E. Pun, J. Li, *J. Mater. Chem.* **2010**, *20*, 7526-7529.

[47] R. F. Service, *Science* **2015**, *348*, 490-492.

[48] A. Y. W. Sham, S. M. Notley, *Soft Matter* **2013**, *9*, 6645-6653.

[49] L. Cheng, C. Yuan, S. Shen, X. Yi, H. Gong, K. Yang, Z. Liu, *ACS Nano* **2015**, *9*, 11090-11101.

[50] B. Zhou, B. Shi, D. Jin, X. Liu, *Nat. Nanotechnol.* **2015**, *10*, 924-936.

[51] T. He, W. Wei, L. Ma, R. Chen, S. Wu, H. Zhang, Y. Yang, J. Ma, L. Huang, G. G. Gurzadyan, H. Sun, *Small* **2012**, *8*, 2163-2168.

[52] Z. Bian , C. Huang , in *Electroluminescence Based on Lanthanide Complexes, in Rare Earth Coordination Chemistry: Fundamentals and Applications* (ed: C. Huang), John Wiley & Sons, Ltd , Chichester, UK **2010** , Ch.11.

[53] M.-K. Tsang, W. Ye, G. Wang, J. Li, M. Yang, J. Hao, *ACS Nano* **2016**, *10*, 598.

[54] a) W. W. Ye, M.-K. Tsang, X. Liu, M. Yang, J. Hao, *Small* **2014**, *10*, 2390; b) H.-T. Wong, M.-K. Tsang, C.-F. Chan, K.-L. Wong, B. Fei, J. Hao, *Nanoscale* **2013**, *5*, 3465; c) S. Zeng, M.-K. Tsang, C.-F. Chan, K.-L. Wong, B. Fei, J. Hao, *Nanoscale* **2012**, *4*, 5118; d) Q. Ju, D. Tu, Y. Liu, R. Li, H. Zhu, J. Chen, Z. Chen, M. Huang, X. Chen, *J. Am. Chem. Soc.* **2012**, *134*, 1323.

[55] Y. Lu, J. Zhao, R. Zhang, Y. Liu, D. Liu, E. M. Goldys, X. Yang, P. Xi, A. Sunna, J. Lu, Y. Shi, R. C. Leif, Y. Huo, J. Shen, J. a. Piper, J. P. Robinson, D. Jin, *Nat. Photonics* **2013**, *8*, 32

[56] J.-N. Liu, W.-B. Bu, J.-L. Shi, *Acc. Chem. Res.* **2015**, *48*, 1797.

[57] a) J. Liu, W. Bu, S. Zhang, F. Chen, H. Xing, L. Pan, L. Zhou, W. Peng, J. Shi, *Chem. Eur. J.* **2012**, *18*, 2335. b) S. Gai, P. Yang, C. Li, W. Wang, Y. Dai, N. Niu, J. Lin, *Adv. Funct. Mater.* **2010**, *20*, 1166. c) X. Zhang, P. Yang, Y. Dai, P. Ma, X. Li, Z. Cheng, Z. Hou, X. Kang, C. Li, J. Lin, *Adv. Funct. Mater.* **2013**, *23*, 4067.

[58] J. Liu, J. Bu, W. Bu, S. Zhang, L. Pan, W. Fan, F. Chen, L. Zhou, W. Peng, K. Zhao, J. Du, J. Shi, *Angew. Chem. Int. Ed.* **2014**, *53*, 4551.

[59] W. Cheng, F. Rechberger, M. Niederberger, *ACS Nano* **2016**, *10*, 2467.

[60] L. Tao, W. Xu, Y. Zhu, L. Xu, H. Zhu, Y. Liu, S. Xu, P. Zhou, H. Song, *J. Mater. Chem. C* **2014**, *2*, 4186.

[61] J. Zhao, D. Jin, E. P. Schartner, Y. Lu, Y. Liu, A. V Zvyagin, L. Zhang, J. M. Dawes, P. Xi, J. a Piper, E. M. Goldys, T. M. Monro, *Nat. Nanotechnol.* **2013**, *8*, 729.

[62] a) G. Chen, H. Qiu, P. N. Prasad, X. Chen, *Chem. Rev.* **2014**, *114*, 5161; b) A. Sedlmeier, H. H. Gorris, *Chem. Soc. Rev.* **2014**; c) X. Chen, D. Peng, Q. Ju, F. Wang, *Chem. Soc. Rev.* **2014**; d) V. Muhr, S. Wilhelm, T. Hirsch, O. S. Wolfbeis, *Acc. Chem. Res.* **2014**, *47*, 3481.

[63] Y. Cui, B. Chen, G. Qian, *Coordin. Chem. Rev.* **2014**, *273*, 76-86.

[64] J. Wang, C. Yan, K. J. Chee, P. S. Lee, *Adv. Mater.* **2015**, *27*, 2876-2882.

[65] L. Chen, M.-C. Wong, G. Bai, W. Jie, J. Hao, *Nano Energy* **2015**, *14*, 372-381.

[66] X. Zhai, S. Liu, X. Liu, F. Wang, D. Zhang, G. Qin, W. Qin, *J. Mater. Chem. C* **2013**, *1*, 1525-1530.

[67] Y. Molard, C. Labbé, J. Cardin, S. Cordier, *Adv. Funct. Mater.* **2013**, *23*, 4821-4825.

[68] S. Watanabe, T. Asanuma, T. Sasahara, H. Hyodo, M. Matsumoto, K. Soga, *Adv. Funct. Mater.* **2015**, *25*, 4390-4396.

[69] R. Deng, F. Qin, R. Chen, W. Huang, M. Hong, X. Liu, *Nature Nanotechnology* **2015**, *10*, 237-242.

[70] S. M. Jeong, S. Song, K.-I. Joo, J. Kim, S.-H. Hwang, J. Jeong, H. Kim, *Energy Environ. Sci.* **2014**, *7*, 3338-3346.

[71] X. Y. Huang, S. Y. Han, W. Huang, X. G. Liu, *Chem. Soc. Rev.* **2013**, *42*, 173-201.

[72] M. Grätzel, *Nature* **2001**, *414*, 338.

[73] X. Wu, G. Q. Max Lu, L. Wang, *Adv. Energy Mater.* **2013**, *3*, 704-707.

[74] M. Luoshan, M. Li, X. Liu, K. Guo, L. Bai, Y. Zhu, B. Sun, X. Zhao, *J. Power Sources* **2015**, *287*, 231-236.

[75] X. Wu, S. Yin, Q. Dong, B. Liu, Y. Wang, T. Sekino, S. W. Lee, T. Sato, *Sci. Rep.* **2013**, *3*, 2918.

[76] Z. Xu, M. Quintanilla, F. Vetrone, A. O. Govorov, M. Chaker, D. Ma, *Adv. Funct. Mater.* **2015**, *25*, 2950-2960.

[77] X. Wu, Y. Zhang, K. Takle, O. Bilsel, Z. Li, H. Lee, Z. Zhang, D. Li, W. Fan, C. Duan, E. M. Chan, C. Lois, Y. Xiang, G. Han, *ACS Nano* **2016**, *10*, 1060-1066.

[78] a) J. Rieffel, U. Chitgupi, J. F. Lovell, *Small* **2015**, *11*, 4445-4461; b) K. Licha, *Top. Curr. Chem.* **2002**, *222*, 1-29; c) G. Hong, S. Diao, J. Chang, A. L. Antaris, C. Chen, B. Zhang, S. Zhao, D. N. Atochin, P. L. Huang, K. I. Andreasson, C. J. Kuo, H. Dai, *Nat. Photon.* **2014**, *8*, 723-730.

[79] a) S. Zeng, M.-K. Tsang, C.-F. Chan, K.-L. Wong, J. Hao, *Biomaterials* **2012**, *33*, 9232; b) H. Xing, W. Bu, S. Zhang, X. Zheng, M. Li, F. Chen, Q. He, L. Zhou, W. Peng, Y. Hua, J. Shi, *Biomaterials* **2012**, *33*, 1079; c) C. Chen, N. Kang, T. Xu, D. Wang, L. Ren, X. Guo, *Nanoscale* **2015**, *7*, 5249; d) Z. Yi, W. Lu, H. Liu, S. Zeng, *Nanoscale* **2015**, *7*, 542; e) C. Liu, Z. Gao, J. Zeng, Y. Hou, F. Fang, Y. Li, R. Qiao, L. Shen, *ACS Nano* **2013**, *7*, 7227.

[80] J. Zhou, M. Yu, Y. Sun, X. Zhang, X. Zhu, Z. Wu, D. Wu, F. Li, *Biomaterials* **2011**, *32*, 1148.

[81] Y. Sun, X. Zhu, J. Peng, F. Li, *ACS Nano* **2013**, *7*, 11290.

[82] S. K. Maji, S. Sreejith, J. Joseph, M. Lin, *Adv. Mater.* **2014**, *26*, 5633.

[83] J. Rieffel, F. Chen, J. Kim, G. Chen, W. Shao, S. Shao, U. Chitgupi, R. Hernandez, S. a Graves, R. J. Nickles, P. N. Prasad, C. Kim, W. Cai, J. F. Lovell, *Adv. Mater.* **2015**, *27*, 1785.

[84] a) J. Xu, S. Zhou, D. Tu, W. Zheng, P. Huang, R. Li, Z. Chen, M. Huang, X. Chen, *Chem. Sci.* **2016**; b) Y. Xi, Z. Chang, X. Ye, H. Huang, Y. Huang, Q. Xiao, H. Lin, *Nanoscale* **2016**, *8*, 1288; c) E.-J. Jo, H. Mun, M.-G. Kim, *Anal. Chem.* **2016**, *88*, 2742.

[85] W. Zheng, P. Huang, D. Tu, E. Ma, H. Zhu, X. Chen, *Chem. Soc. Rev.* **2015**, *44*, 1379.

[86] S. Xu, B. Dong, D. Zhou, Z. Yin, S. Cui, W. Xu, B. Chen, H. Song, *Sci. Rep.* **2016**, *6*, 23406.

[87] H. Guo, N. M. Idris, Y. Zhang, *Langmuir* **2011**, *27*, 2854-2860.

[88] Y. Zhou, W. Pei, C. Wang, J. Zhu, J. Wu, Q. Yan, L. Huang, W. Huang, C. Yao, J. S. C. Loo, Q. Zhang, *Small* 2014, *10*, 3560-3567.

[89] Y. Liu, M. Chen, T. Cao, Y. Sun, C. Li, Q. Liu, T. Yang, L. Yao, W. Feng, F. Li, *J. Am. Chem. Soc.* **2013**, *135*, 9869-9876.

[90] F. M. Kievit, M. Zhang, *Adv. Mater.* **2011**, *23*, 217.

[91] a) P. Padhye, A. Alam, S. Ghorai, S. Chattopadhyay, P. Poddar, *Nanoscale* **2015**, *7*, 19501; b) G. Tian, Z. Gu, L. Zhou, W. Yin, X. Liu, L. Yan, S. Jin, W. Ren, G. Xing, S. Li, Y.

Zhao, *Adv. Mater.* **2012**, *24*, 1226; c) C. Wang, L. Cheng, Z. Liu, *Biomaterials* **2011**, *32*, 1110; d) L. Zhou, X. Zheng, Z. Gu, W. Yin, X. Zhang, L. Ruan, Y. Yang, Z. Hu, Y. Zhao, *Biomaterials* **2014**, *35*, 7666; e) W. Song, W. Di, W. Qin, *Dalt. Trans.* **2016**.

[92] Y. Yang, B. Velmurugan, X. Liu, B. Xing, *Small* 2013, 9, 2937-2944.

[93] Y. Dai, H. Xiao, J. Liu, Q. Yuan, P. a. Ma, D. Yang, C. Li, Z. Cheng, Z. Hou, P. Yang, J. Lin, *J. Am. Chem. Soc.* **2013**, *135*, 18920-18929.

[94] a) Z. Li, Y. Zhang, X. Wu, L. Huang, D. Li, W. Fan, G. Han, *J. Am. Chem. Soc.* **2015**, *137*, 5304; b) Z. Li, Y. Zhang, X. Wu, X. Wu, R. Maudgal, H. Zhang, G. Han, *Adv. Sci.* **2015**, *2*, 1500001; c) Z. Li, H. Zhang, M. Sun, J. Shen, H. Fu, *J. Mater. Chem.* **2012**, *22*, 24713-24720.

[95] J. Shi, X. Sun, J. Li, H. Man, J. Shen, Y. Yu, H. Zhang, *Biomaterials* **2015**, *37*, 260.

[96] C. Wang, H. Tao, L. Cheng, Z. Liu, *Biomaterials* **2011**, *32*, 6145.

[97] L. Cheng, K. Yang, Y. Li, J. Chen, C. Wang, M. Shao, S.-T. Lee, Z. Liu, *Angew. Chem. Int. Ed.* **2011**, *123*, 7523.

[98] D. K. Chatterjee, Y. Zhang, *Nanomedicine* **2008**, *3*, 73.

[99] N. M. Idris, M. K. Gnanasammandhan, J. Zhang, P. C. Ho, R. Mahendran, Y. Zhang, *Nat. Med.* **2012**, *18*, 1580.

[100] S. Cui, D. Yin, Y. Chen, Y. Di, H. Chen, Y. Ma, S. Achilefu, Y. Gu, *ACS Nano* **2013**, *7*, 676.

[101] a) X. Huang, I. H. El-Sayed, W. Qian, M. A. El-Sayed, *J. Am. Chem. Soc.* **2006**, *128*, 2115; b) E. B. Dickerson, E. C. Dreaden, X. Huang, I. H. El-Sayed, H. Chu, S. Pushpanketh, J. F. McDonald, M. A. El-Sayed, *Cancer Lett.* **2008**, *269*, 57.

[102] L. Cheng, K. Yang, Y. Li, X. Zeng, M. Shao, S.-T. Lee, Z. Liu, *Biomaterials* **2012**, *33*, 2215.

[103] B. Dong, S. Xu, J. Sun, S. Bi, D. Li, X. Bai, Y. Wang, L. Wang, H. Song, *J. Mater. Chem.* **2011**, *21*, 6193.

[104] Y. Wang, H. Wang, D. Liu, S. Song, X. Wang, H. Zhang, *Biomaterials* **2013**, *34*, 7715.

[105] A. Stevenson, A. Jones, S. Raghavan, *Nano Lett.* **2011**, *11*, 3274-3278.

[106] X. Wang, H. Zhang, R. Yu, L. Dong, D. Peng, A. Zhang, Y. Zhang, H. Liu, C. Pan, Z. L. Wang, *Adv. Mater.* **2015**, *27*, 2324-2331.

[107] M. L. Debasu, D. Ananias, I. Pastoriza-Santos, L. M. Liz-Marzán, J. Rocha, L. D. Carlos, *Adv. Mater.* **2013**, *25*, 4868-4874.

[108] C. D. Brites, P. P. Lima, N. J. Silva, A. Millán, V. S. Amaral, F. Palacio, L. D. Carlos, *Adv. Mater.* **2010**, *22*, 4499-4504.

[109] J. Dong, J. I. Zink, *ACS nano* **2014**, *8*, 5199-5207.

[110] M. Ramirez, D. Jaque, L. Bausa, I. Martin, F. Lahoz, E. Cavalli, A. Speghini, M. Bettinelli, *J. Appl. Phys.* **2005**, *97*, 093510.

[111] M.-C. Wong, L. Chen, M.-K. Tsang, Y. Zhang, J. Hao, *Adv. Mater.* **2015**, *27*, 4488-4495.

[112] O. Graydon, *Nat. Photonics*, **2015**, *9*, 558.

[113] C.-W. Yeh, Y.-P. Liu, Z. R. Xiao, Y.-K. Wang, S.-F. Hu, R.-S. Liu, *J. Mater. Chem.* **2012**, *22*, 5828.

Figure captions

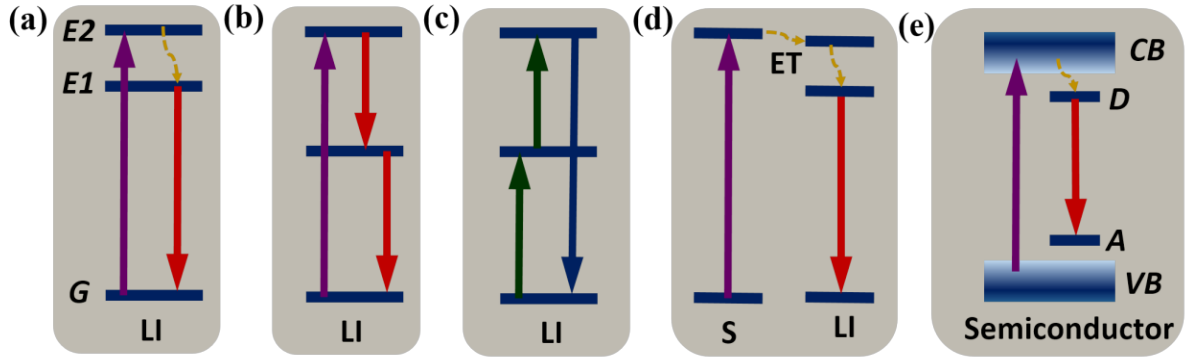

Figure 1. Luminescent ions upon excitation. (a) Down-shifting process. (b) Down-conversion process. (c) Upconversion process. (d) Sensitized emission from an activator through energy transfer. (e) Emission from a luminescent ion doped semiconductor after band-to-band excitation. The upward and downward arrows denote the excitation and emission, respectively. The dashed line denotes a non-radiative relaxation process. LI represents luminescent ions. E and G represent the excited and ground states of the luminescent ions, respectively. S is a sensitizer. ET means the energy transfer. CB and VB denote the conduction and valence bands of the metal-ion-doped semiconductor, while D and A represent the donor and acceptor energy levels, respectively.

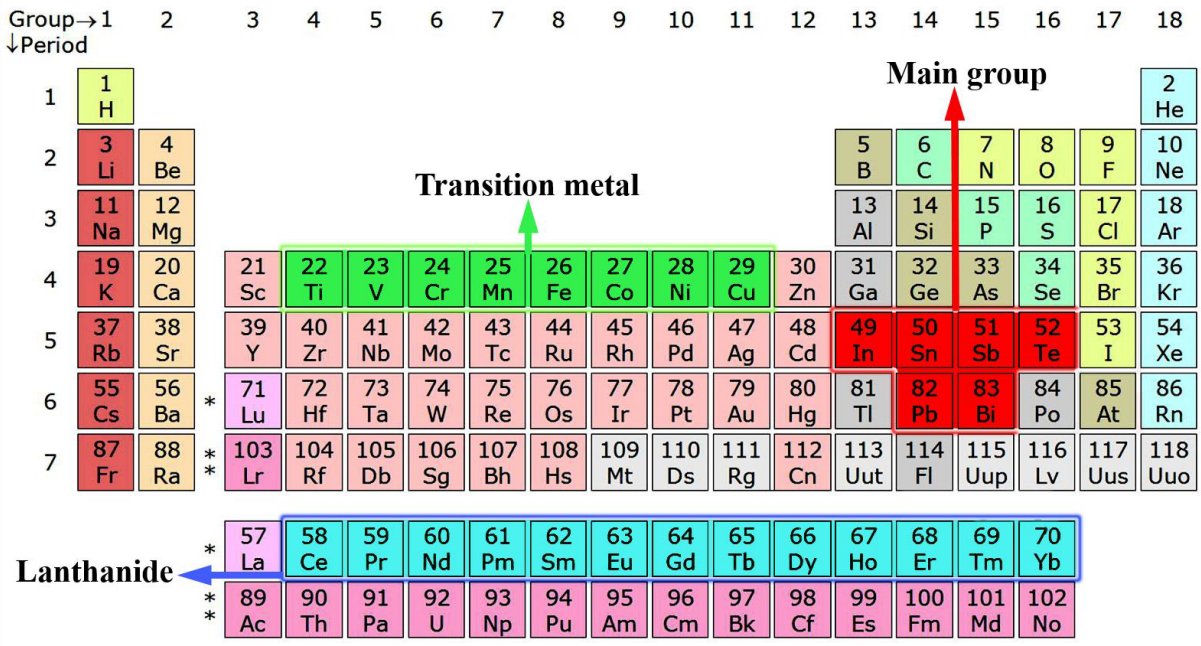

Figure 2. The luminescent ions are highlighted in the periodic table.

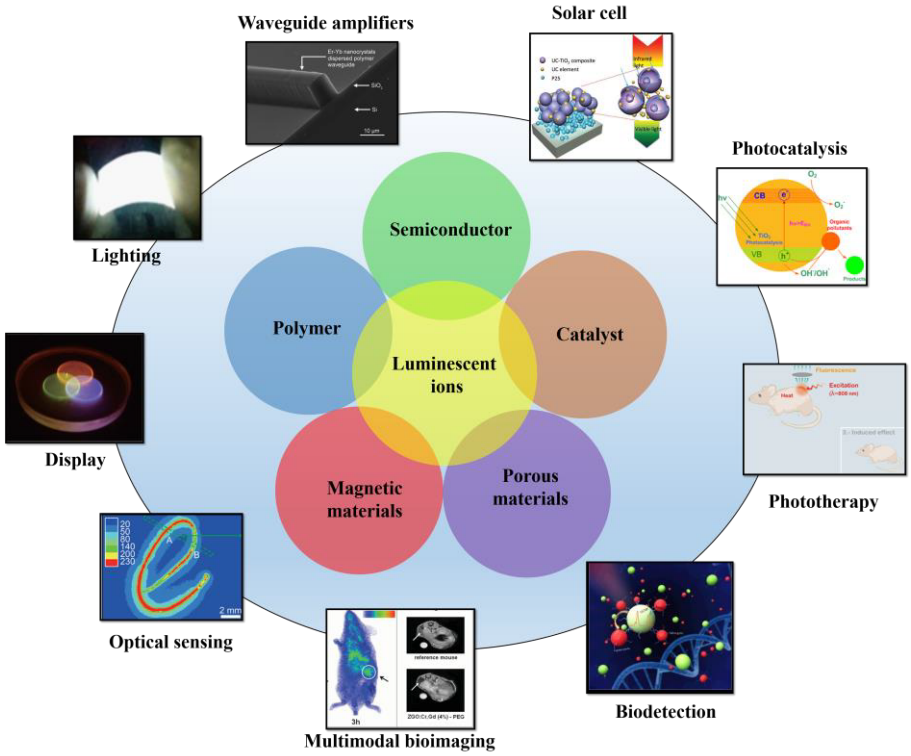

Figure 3. Incorporating luminescent ions into advanced functional materials.

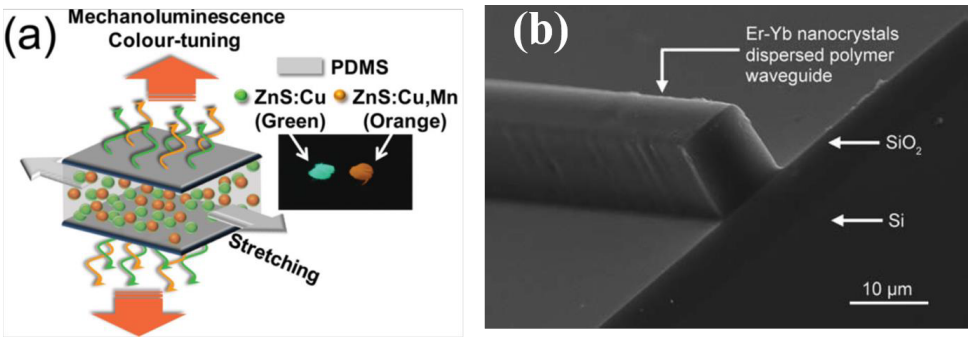

Figure 4. (a) Schematic illustration of the color tunable mechanoluminescent metal-ion-doped ZnS-polymer matrix composite films. Copyright 2013, Wiley-VCH. Reproduced with permission.[45] (b) A tilted SEM image of the as-prepared Er-Yb doped NPs dispersed polymer composite waveguide amplifier. Copyright 2010, Royal Society of Chemistry. Reproduced with permission.[46]

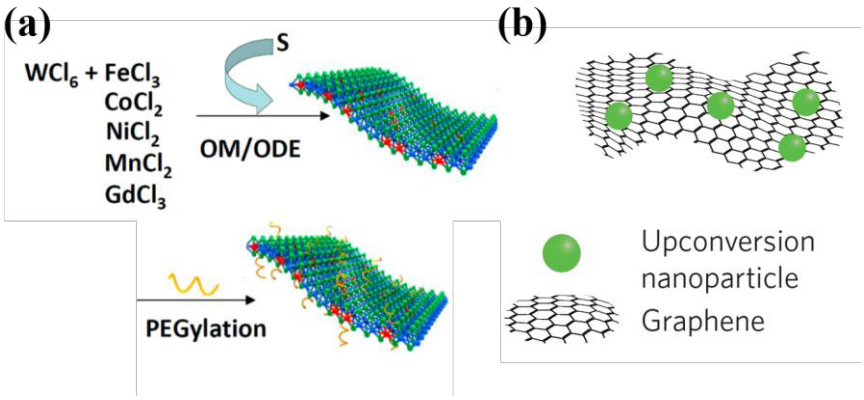

Figure 5. (a) Scheme showing the bottom-up synthesis of metal-ion-doped WS_2 nanoflakes. Copyright 2015, American Chemical Society. Reproduced with permission. [49] (b) Combining graphene nanosheets with rare-earth-ions doped upconversion NPs. Copyright 2015, Nature Publishing Group. Reproduced with permission.[50]

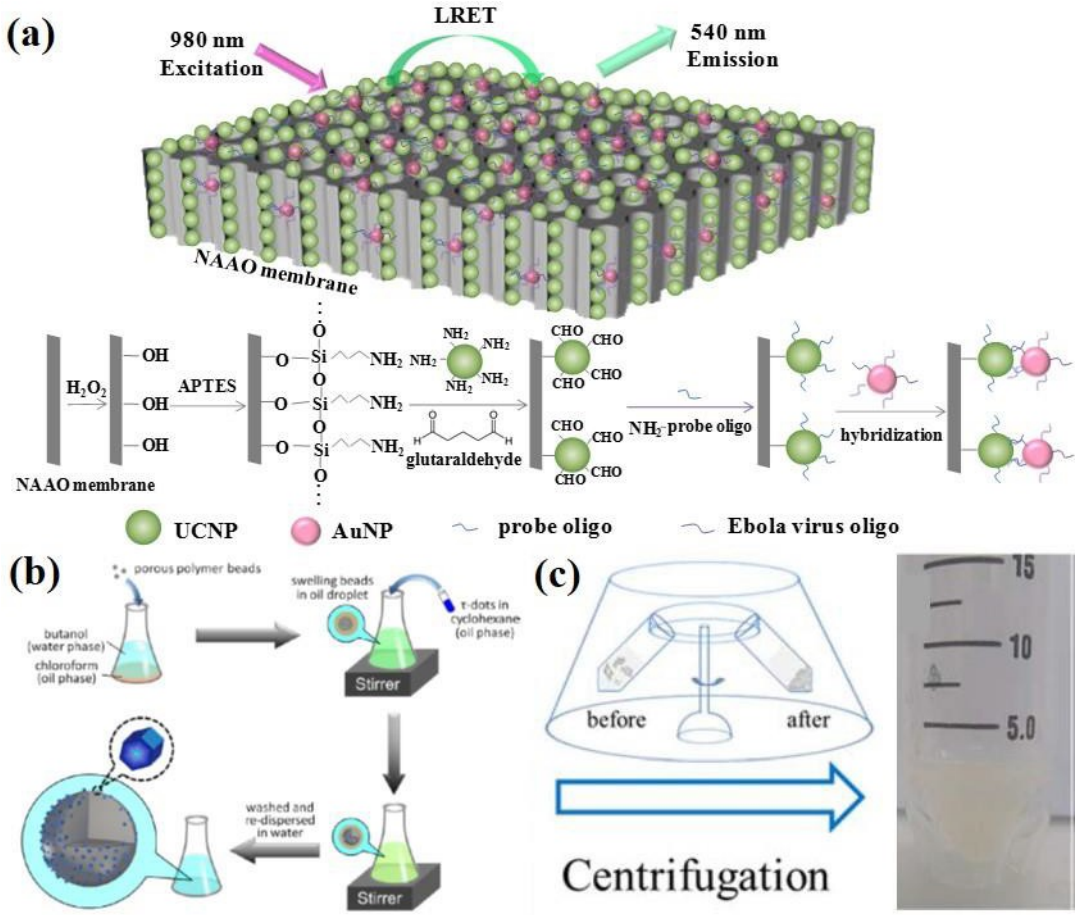

Figure 6 (a) Functionalization of NAAO and the subsequent anchoring of amine-functionalized UCNPs into the hollow channels of NAAO. Copyright 2016, American Chemical Society. Reproduced with permission.[53] (b) Preparation of porous luminescent composite by utilizing the hydrophobic-hydrophobic interaction of oleate UCNPs and swelled PS microspheres. Copyright 2013, Nature Publishing Group. Reproduced with permission. [61] (c) Formation of Y_2O_3 nanosheets gel after centrifugation. Copyright 2016, American Chemical Society. Reproduced with permission. [59]

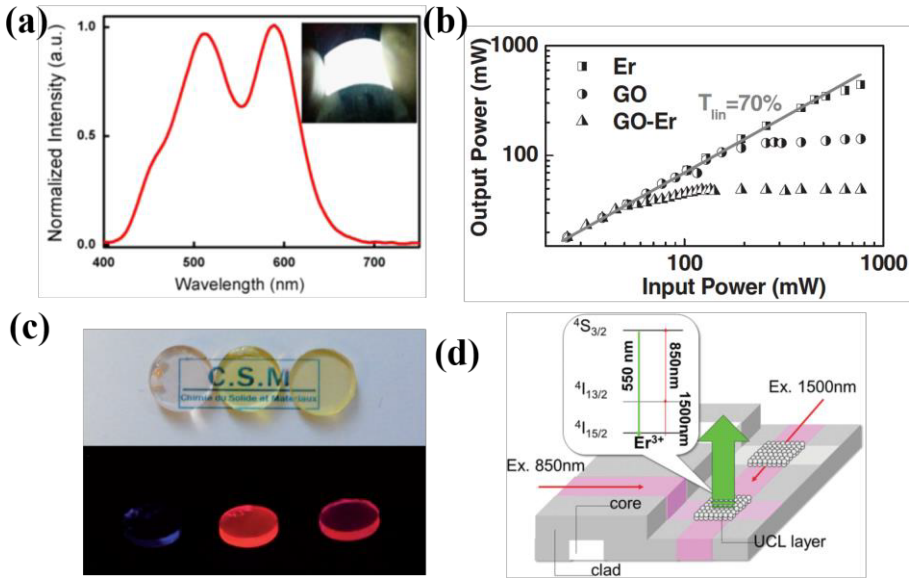

Figure 7. (a) Luminescence spectrum of the flexible composite device biased at 100 V and 1 kHz. The inset presents the photograph of white light-emission. Copyright 2015, Elsevier. Reproduced with permission. [65] (b) Optical limiting response of $NaYF_4:Yb^{3+}/Er^{3+}$, GO, and $GO/NaYF_4:Yb^{3+}/Er^{3+}$ solutions. Copyright 2012, Wiley-VCH. Reproduced with permission. [51] (c) Digital photos of the Er^{3+} doped PMMA composite pellets under visible (top) and UV light (bottom, A_{ex}=365 nm); with Er^{3+} complexes (1.3, 0.5, 1.3 wt %) from left to right; the right two with Mo_6 cluster. Copyright 2013, Wiley-VCH. Reproduced with permission. [67] (d) Illustration of arrayed waveguide gratings-upconversion luminescent devices for the fabrication of flexible transparent displays. Copyright 2015, Wiley-VCH. Reproduced with permission. [68]

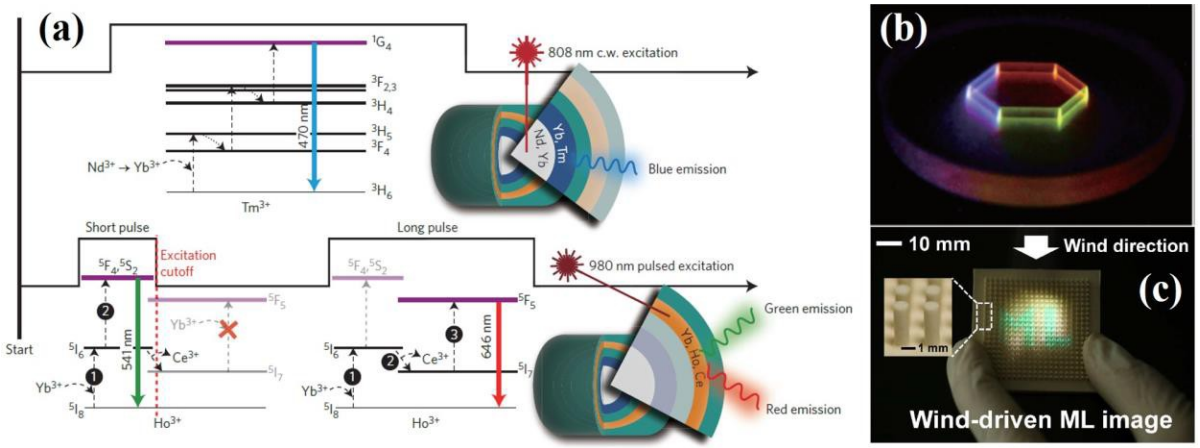

Figure 8. Schematic illustration of temporal multicolour emission in $NaYF_4$-based core-shell nanocrystals under c.w. and pulse excitation. (b) Full-colour volumetric 3D display using a composite based pulse-duration-sensitive luminescent ion doped NPs. Copyright 2015, Nature Publishing Group. Reproduced with permission. [69] (c) Harnessing wind-driven display based on luminescent ion doped mechanoluminescence (ML) composite. Copyright 2014, Royal Society of Chemistry. Reproduced with permission. [70]

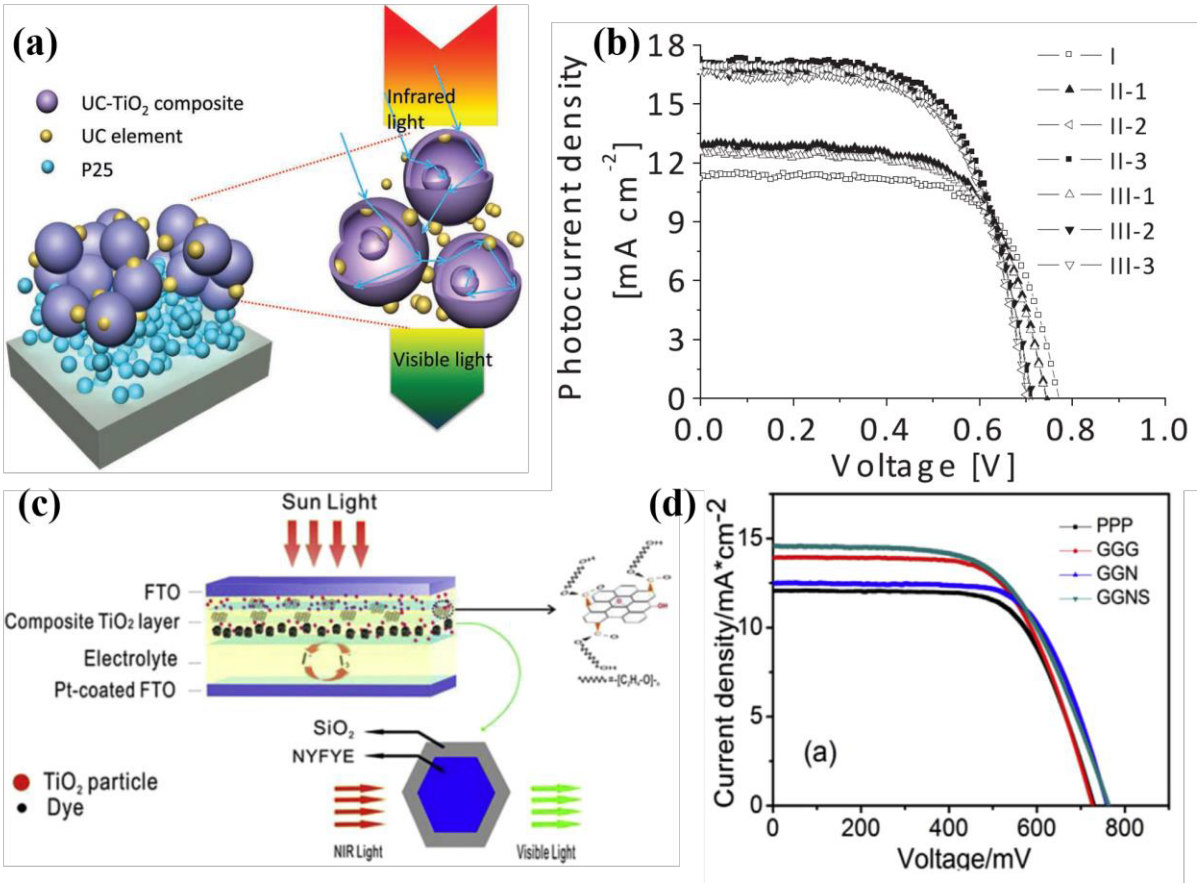

Figure 9. Ln^{3+} doped upconversion NPs-TiO_2 composite dye-sensitized solar cells (DSSCs). (a) Schematic of the thin film with TiO_2 (P25) particles as under-layer and upconversion NPs-TiO_2 composites as top layer. (b) Performance of the prepared cells. Copyright 2013, Wiley-VCH. Reproduced with permission. [73] (c) Schematic structure of the DSSC incorporated with core-shell NYFYE@SiO_2 and graphene in the composite of TiO_2 film, along with graphene oxide (up-right corner) and the cross section of a NYFYE@SiO2 hexagonal prism and the schematic of the upconversion process (lower part). (d) Performance of the prepared DSSCs with different photoanodes. Copyright 2015, Elsevier. Reproduced with permission. [74]

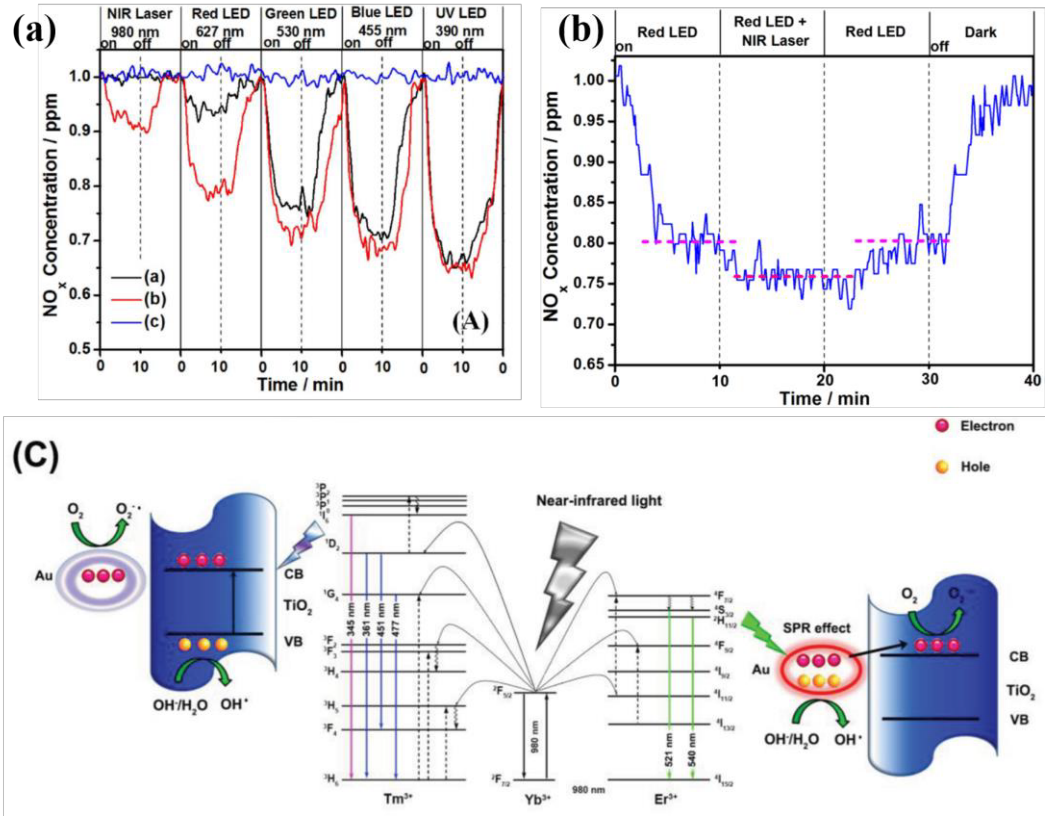

Figure 10. (a) Time dependence of NO_x destruction activity of C-TiO_2 (black), (1:1)@(Yb,Er)-$NaYF_4$/C-TiO_2 (red), (Yb,Er)-$NaYF_4$ (blue) (b) DeNO_x ability of composite (1:1)@(Yb,Er)-$NaYF_4$/C-TiO_2 with response to the different irradiation lights. Copyright 2013, Nature Publishing Group. Reproduced with permission. [75] (c) Schematic illustration of the photocatalysis mechanisms under NIR irradiation. Copyright 2015, Wiley-VCH. Reproduced with permission. [76]

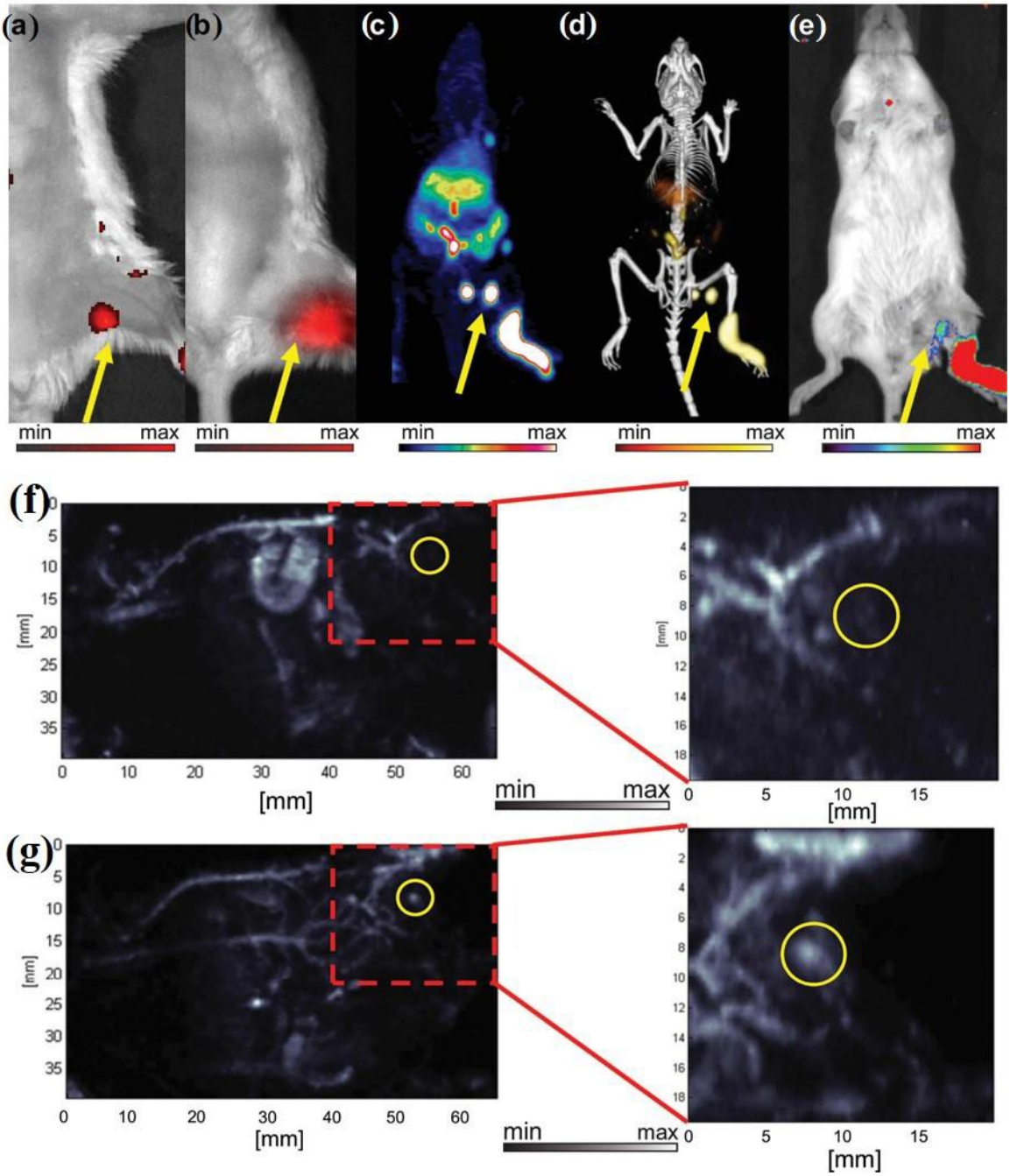

Figure 11. In *vivo* lymphatic imaging using PoP-UCNPs in mice. PoP-UCNPs were injected in the rear left footpad and imaged in six modalities 1 h post-injection. Accumulation of PoP-UCNPs in the first draining lymph node is indicated with yellow arrows. (a) Traditional FL and (b) UCL images with the injection site cropped out of frame. (c) Full anatomy PET, (d) merged PET/CT, and (e) CL images. (f) PA images before and (g) after injection showing endogenous PA blood signal compared to the contrast enhancement that allowed visualization

of the previously undetected lymph node. Copyright 2015, Wiley-VCH. Reproduced with permission. [83]

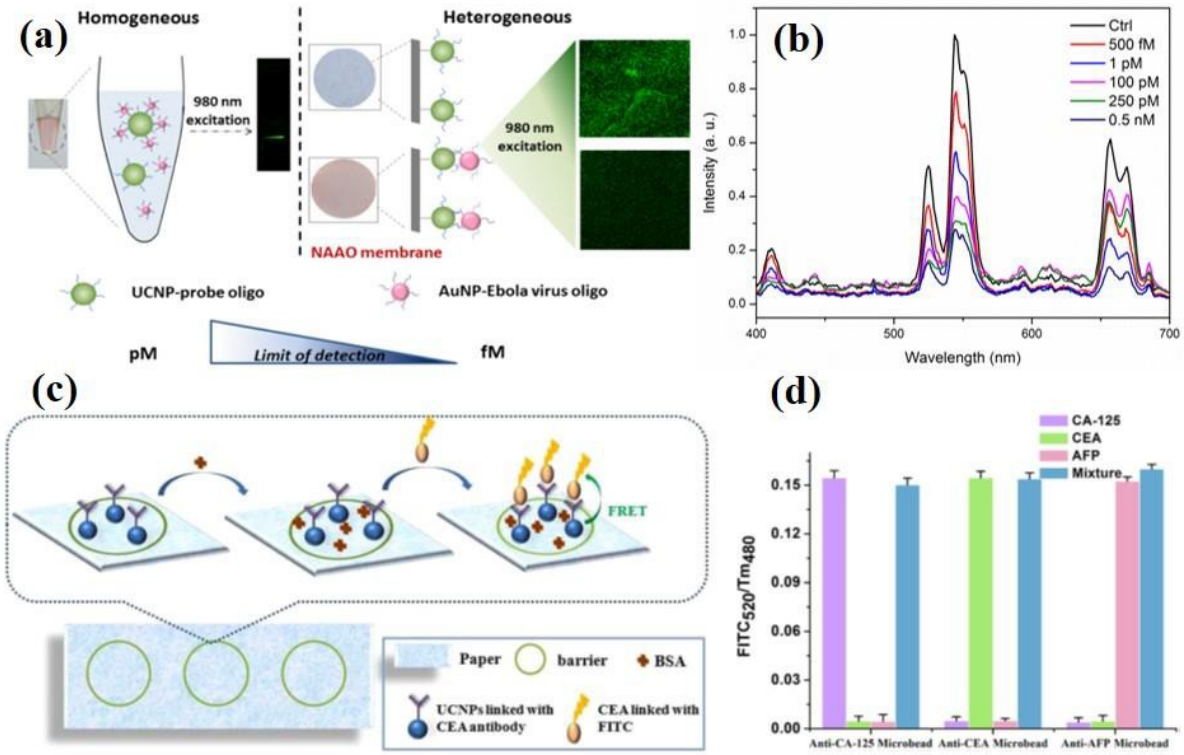

Figure 12. (a) Comparison of the homogeneous and heterogeneous assays for Ebola virus oligo detection; (b) UCL spectra of Ebola clinical sample detection. Notice that the LOD of the detection system can be improved from pM to fM level by the use of NAAO membrane. Copyright 2016, American Chemical Society. Reproduced with permission.[53] (c) The structure of the LRET paper device based on UCNPs and FITC; (d) Changes in luminescent intensity in the presence of the mixture of three cancer biomarkers. Copyright 2016, Nature Publishing Group. Reproduced with permission. [86]

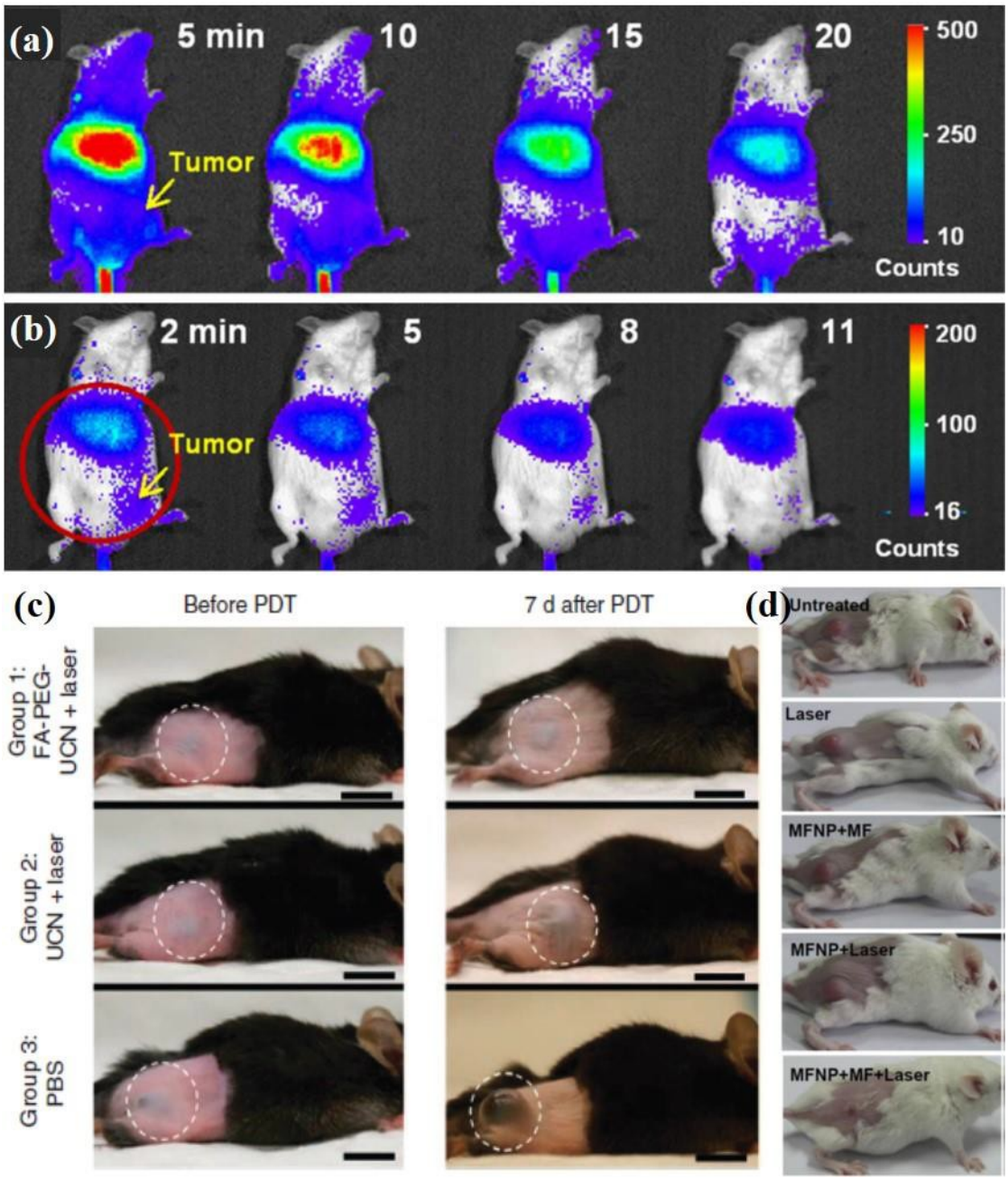

Figure 13. (a) *In vivo* luminescence images of H22 tumor-bearing mice after intravenous injection of the (FA) modified-$Zn_{1.1}Ga_{1.8}Ge_{0.1}O_4:Cr^{3+}$, Eu^{3+} @SiO_2 with DOX loading. (b) Secondary excitation by red LED for 2 min after 2 h of circulation. The yellow arrow in the figure indicates the tumor site. Copyright 2015, Elsevier. Reproduced with permission. [95] (c) Photos of the mouse in testing group 1, 2 and 3 intravenously injected with FA-PEG-UCNPs, unmodified UCNPs or PBS showing the change in tumor size. Copyright 2012, Nature Publishing Group. Reproduced with permission. [99] (d) Representative photos of 4T1 tumor

bearing mice in different test groups with different treatment. Copyright 2012, Elsevier. Reproduced with permission. [102]

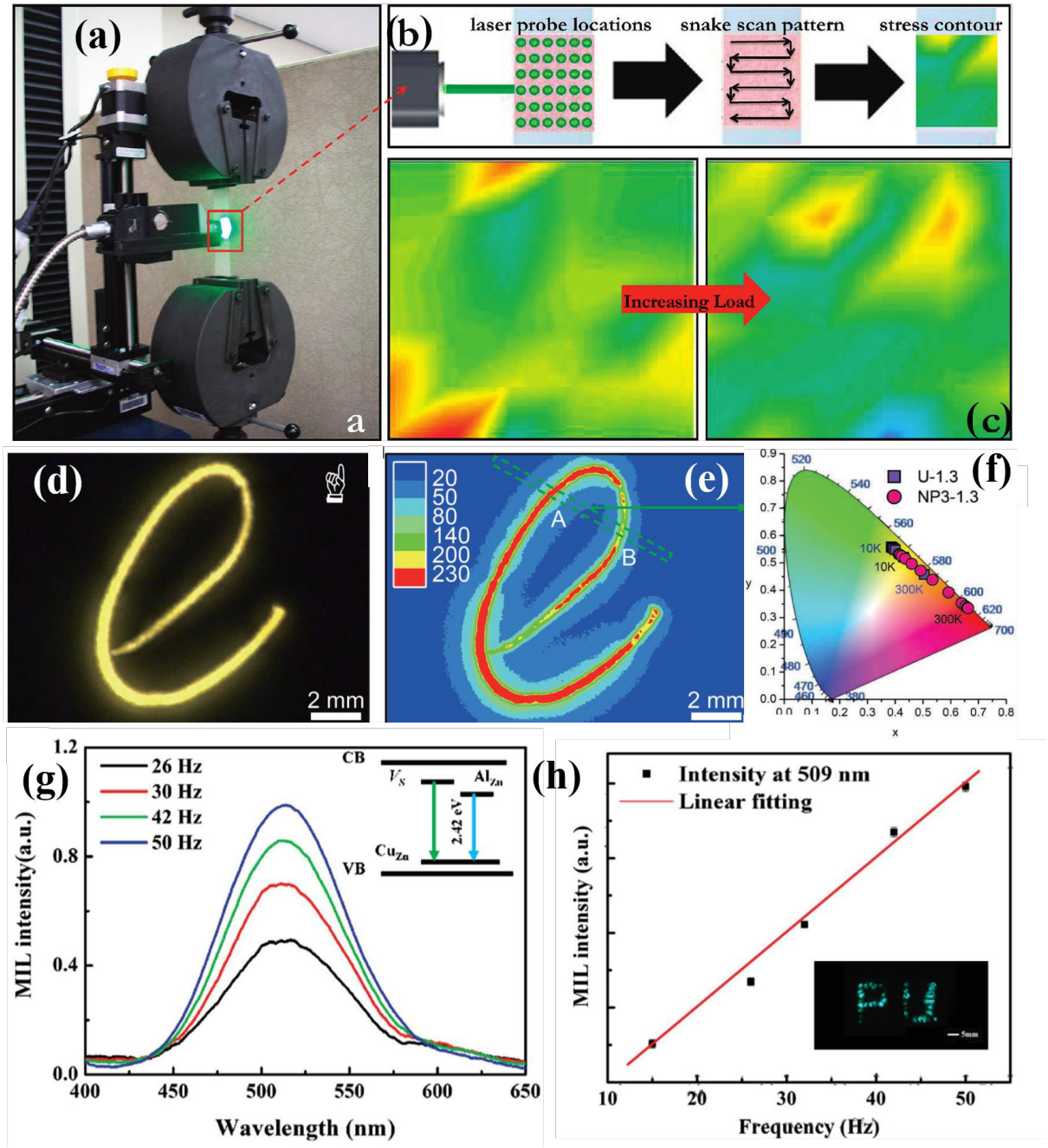

Figure 14. Sensor application of luminescent composites. (a) Stress-sensing adhesive application in a single lap-shear configuration. (b) A stress-spectral mapping. (c) Stress distribution with increasing load through contour maps of R1 peak positions from Cr^{3+} ions. Copyright 2011, American Chemical Society. Reproduced with permission.[105] (d) Visualized pressure distributions produced from a hand ritten "e". (e) The corresponding 2D mapping of luminescence intensity from (d). Copyright 2015, Wiley-VCH. Reproduced with permission. [106] (f) CIE chromaticity diagram presenting the temperature dependence of the (x,y) color

coordinates of nanocomposites. Copyright 2010, Wiley-VCH. Reproduced with permission.[108] (g) Luminescence spectra of Al,Cu-doped ZnS phosphor mixed with Fe-Co-Ni and PDMS composite laminate activated by ac magnetic field. The inset shows the energy level diagram. (h) MIL intensity at 509 nm measured from Al,Cu-doped ZnS-based composite as a function of frequency under ac magnetic field. The inset shows photograph of displaying green colored logo "PU" from MIL materials driven b lo magnetic field. Copyright 2015, Wiley-VCH. Reproduced with permission.[111]

Tables

Table 1 Typical luminescent ions and their emissions corrosponded to energy transitions

Types	Ions	Emissions J_{em} (nm)	Corresponding energy transitions	Examples	References
Lanthanide (Ln)	Yb^{3+}	950-1050	$^2F_{5/2}$ $^2F_{7/2}$	$NaYbF_4$: Yb^{3+}; GdF_3: Yb^{3+}, J_{em}=980 nm	[11]
	Tm^{3+}	450, 475, 644, 800, 1750-1900	$^1D_2$ $^3F_4$, $^1G_4$ $^3H_6$, $^1G_4$ $^3F_4$, $^3H_4$ $^3H_6$, $^3F_4$ $^3H_6$	$BaTiO_3$: Tm^{3+}, J_{em}=450, 475, 644, 800 nm	[12]
	Er^{3+}	525, 542, 655, 980, 1540	$^2H_{11/2}$ $^4I_{15/2}$, $^4S_{3/2}$ $^4I_{15/2}$, $^4F_{9/2}$ $^4I_{15/2}$, $^4I_{11/2}$ $^4I_{15/2}$, $^4I_{13/2}$ $^4I_{15/2}$	Er^{3+} doped germanate glass, J_{em}=525, 542, 655, 980, 1540 nm	[13]
	Ho^{3+}	542, 655, 1980-2100	$^5F_4$, $^5S_2$ $^5I_8$, $^5F_5$ $^5I_8$, $^5I_7$ $^5I_8$	Ba_2YbF_7: Ho^{3+}, J_{em}=542, 655, 2050 nm	[14]
	Eu^{3+}	620	$^5D_0$ ^7F_J (J=0-6)	$NaGdF_4$: Eu^{3+}, J_{em}=620 nm	[15]
	Nd^{3+}	1064	$^4F_{3/2}$ $^4I_{11/2}$	Ga_2O_3: Nd^{3+}, J_{em}=620 nm	[16]
	Tb^{3+}	381, 415, 438, 489, 541, 584, 619	$^5D_3$ ^7F_J, (J=6-4), $^5D_4$ ^7F_J, (J=6-3)	$Sr_2B_5O_9Cl$: Tb^{3+}, J_{em}=546 nm	[17]
	Sm^{3+}	520, 541, 555, 590, 646, 657	$^4G_{7/2}$ $^6H_{5/2}$, $^4F_{3/2}$ $^6H_{5/2}$, $^4G_{5/2}$ $^6H_{5/2}$, $^4G_{5/2}$ $^6H_{7/2}$, $^4G_{7/2}$ $^6H_{9/2}$, $^4G_{5/2}$ $^6H_{9/2}$	$Sr_{n+1}Sn_nO_{3n+1}$: Sm^{3+}, J_{em}=520, 624 nm	[18]
	Pr^{3+}	485, 605, 1300	$^3P_0$ $^3H_4$, $^1D_2$ $^3H_4$, $^1G_4$ $^3H_5$	$Ba_{0.77}Ca_{0.23}TiO_3$: Pr^{3+}, J_{em}=612 nm	[19]
Transition metal (TM)	Cr^{3+}	670-1800	$^4T_2$, ^2E $^4A_2$	$NaAl(WO_4)_2$: Cr^{3+}, J_{em}=700-1150 nm	[20]
	Mn^{2+}	510-630	$^4T_1$ $^6A_1$	$KZnF_3$: Mn^{2+}, J_{em}=585 nm	[21]
	Mn^{4+}	650-730	^2E_g $^4A_2$	K_2TiF_6: Mn^{4+}, J_{em}=650-730 nm, quantum yield ~ 98 %.	[22]
	Ni^{2+}	1000-1800	$^3T_2(^3$) $^3A_2(^3F)$	$Ba_xSr_{1-x}TiO_3$: Ni^{2+}, J_{em}=1100-1650 nm	[23]
Main group	Pb^{2+}	370-380	$^3P_1$ $^1S_0$	Silicate oxyapatites: Pb^{2+} J_{em}=370-380 nm	[24]
	Bi ions	1000-2000	Transitions of Bi species	Bi doped glasses, J_{em}=1100-1700 nm	[25]

Table 2 Material selection for luminescent ions in composite materials design

Material Choices	Example	Merits	Application	References
Polymers	Polydimethylsiloxane (PDMS), poly(methyl methacrylate) (PMMA)	Flexible, easy processabilty, low-cost	Photonic and optoelectronic devices	[38]
Magnetic materials	Fe_3O_4, Fe-Co-Ni alloy	Magnetic properties	Sensors	[39]
Porous materials	Nanoporous anodized alumina membrane (NAAO); mesoporous SiO_2	Small pores, large surface area	Biosensing, drug delivery	[40]
Catalysts	TiO_2	Photocatalyst under UV light	Improved photocatalysis	[41]
2D materials	Grapheme; 2D-layered transition metal dichalcogenides (TMDs)	Atomic layer, large surface area	Optical limiting, phototherapy	[42]

Integrating luminescent ions and advanced materials into multifunctional systems seems to be a tendency, motivated by the stimulating desires of fundamental studies and technological applications. This feature article provides a general overview of luminescent ions-based advanced composite materials recently investigated, which have promising multifunctional applications in a broad area, including optoelectronics, photonics, clean energy, biomedicine, and new types of sensors.

Keyword

Metal ion dopants, luminescence, upconversion nanocrystals, composites, multifunctional applications

G. X. Bai, M.-K. Tsang, Prof. J. H. Hao*

Luminescent ions in advanced composite materials for multifunctional applications